The Influence of Salt on the Structure and Energetics of Supercoiled DNA

Tamar Schlick,*‡ Bin Li,* and Wilma K. Olson§

* New York University, and ‡Howard Hughes Medical Institute, Chemistry Department and Courant Institute of Mathematical Sciences, New York, New York 10012; and §Department of Chemistry, Rutgers, the State University of New Jersey, Wright-Rieman Laboratories, New Brunswick, New Jersey 08903 USA

ABSTRACT We present a detailed computational study of the influence of salt on the configurations, energies, and dynamics of supercoiled DNA. A potential function that includes both elastic and electrostatic energy components is employed. Specifically, the electrostatic term, with salt-dependent coefficients, is modeled after Stigter's pioneering work on the effective diameter of DNA as a function of salt concentration. Because an effective charge per unit length is used, the electrostatic formulation does not require explicit modeling of phosphates and can be used to study long DNAs at any desired resolution of charge. With explicit consideration of the electrostatic energy, an elastic bending constant corresponding to the nonelectrostatic part of the bending contribution to the persistence length is used. We show, for a series of salt concentrations ranging from 0.005 to 1.0 M sodium, how configurations and energies of supercoiled DNA (1000 and 3000 base pairs) change dramatically with the simulated salt environment. At high salt, the DNA adopts highly compact and bent interwound states, with the bending energy dominating over the other components, and the electrostatic energy playing a minor role in comparison to the bending and twisting terms. At low salt, the DNA supercoils are much more open and loosely interwound, and the electrostatic components are dominant. Over the range of three decades of salt examined, the electrostatic energy changes by a factor of 10. The buckling transition between the circle and figure-8 is highly sensitive to salt concentration: this transition is delayed as salt concentration decreases, with a particularly sharp increase below 0.1 M. For example, for a bending-to-twisting force constant ratio of $A/C = 1.5$, the linking number difference (ΔLk) corresponding to equal energies for the circle and figure-8 increases from 2.1 to 3.25 as salt decreases from 1.0 to 0.005 M. We also present in detail a family of three-lobed supercoiled DNA configurations that are predicted by elasticity theory to be stable at low ΔLk. To our knowledge, such three-dimensional structures have not been previously presented in connection with DNA supercoiling. These branched forms have a higher bending energy than the corresponding interwound configurations at the same ΔLk but, especially at low salt, this bending energy difference is relatively small in comparison with the total energy, which is dominated by the electrostatic contributions. Significantly, the electrostatic energies of the three-lobed and (straight) interwound forms are comparable at each salt environment. We show how the three-lobed configurations change slowly with ΔLk, resulting in branched interwound forms at higher salt. In longer chains, the branched forms are highly interwound, with bent arms. At low salt, the branched supercoils are asymmetric, with a longer interwound stem and two shorter arms. From molecular dynamics simulations we observe differences in the motions of the DNA as a function of salt. At high salt, the supercoiled chain is quite compact but fairly rigid, whereas at low salt the DNA is loosely coiled but more dynamic. Especially notable at low salt are the large-scale opening and closing of the chain as a whole and the rapid "slithering" of individual residues past one another. Toroidal forms are not detected under these conditions. However, the overall features of the open, loose supercoils found at low salt are more similar to those of toroidal than interwound configurations. Indeed, simulated x-ray scattering profiles reveal the same trends observed experimentally and are consistent with a change from closed to open forms as salt is decreased. Like the minimization studies, the dynamics reveal a critical point near 0.1 M associated with the collapse of loose to tight supercoils. Near this physiological concentration, enhanced flexibility of the DNA is noted. The collective observations suggest a potential regulatory role for salt on supercoiled DNA function, not only for closed circular DNA, but also for linear DNA with small looped regions.

INTRODUCTION

The long-range effects of electrostatic interactions are recognized as important factors in determining the folding of biopolymers, such as proteins and DNA, their interactions with other molecular species, and their dynamics. Indeed, current improvements in our molecular modeling force field are being sought through consideration of all nonbonded pairwise interactions using fast particle methods (e.g., Greengard, 1988; Shimada et al., 1994). As a polyelectrolyte, DNA is expected to be profoundly affected by ionic interactions in its natural cellular environment. Positive counterions screen the negatively charged phosphate groups along the DNA backbone and thereby permit chain segments to come into intimate contact. The nature of the electrostatic interactions is complex as many competing factors—including chain configuration, ionic concentration, and ion type (size and shape)—are involved (Manning, 1978). For superhelical DNA, salt effects are particularly important because many parts of the double helix that are distant in linear sequence come into close contact upon supercoiling. Nodes of such contacts arise in interwound, branched, knotted, and catenated forms of supercoiled DNA. One can imagine, then, a complex competition between the superhelical-strain forces, on one hand, that tend to bring DNA segments

Received for publication 8 June 1994 and in final form 11 August 1994.

Address reprint requests to Dr. Tamar Schlick, Chemistry Department, New York University and Courant Institute of Mathematical Sci., 251 Mercer Street, New York, NY 10012. Tel.: 212-998-3116; Fax: 212-995-4152; E-mail: schlick@nyu.edu.

0006-3495/94/12/2146/21 $2.00

together—to minimize the elastic energy and increase the magnitude of the writhing number—and the repulsive electrostatic forces and entropic factors, on the other hand, that tend to keep DNA segments apart.

Theoretical treatment of DNA supercoiling is emerging as an important counterpart to experimental work. New understanding of large-scale structure has come from a wide variety of computer simulations, involving Monte Carlo/simulated-annealing techniques (Vologodskii et al., 1979, 1992; Tsuru and Wadati, 1986; Hao and Olson, 1989a, b; Klenin et al., 1989, 1991; Tan and Harvey, 1989, 1991; Olson and Zhang, 1991; Zhang et al., 1991; Fenley et al., 1994), deterministic energy minimization (Schlick and Olson, 1992a; Schlick et al., 1994), finite-element approaches (Yang et al., 1993; Bauer et al., 1993), and Brownian (Chirico and Langowski, 1992), and molecular dynamics methods (Schlick and Olson, 1992a, b; Sprous et al., 1994). For a recent review, see Vologodskii and Cozzarelli, 1994. The typical energy model in these simulations is based on an elastic energy function with bending and twisting components appropriate for an uncharged, isotropic, long thin rod with circular cross section (Love, 1944). The model is conceptually simple and convenient to simulate by computer because the bending and twisting deformations of the supercoiled DNA are expressed in terms of standard geometric quantities of the chain. In addition to information on macromolecular shape, new understanding has also accumulated from these studies on relationships between predicted low energy forms and key physical parameters of superhelical DNA (such as superhelical density, energy constants; Vologodskii and Cozzarelli, 1994).

We are increasingly becoming aware, however, that an adequate treatment of the electrostatic interactions of supercoiled DNA is essential for correctly predicting DNA properties; the commonly used hard-sphere excluded-volume and Lennard-Jones potentials are only coarse approximations of these effects. Just as in all-atom force-fields of proteins and DNA, for supercoiled DNA electrostatics are a major component and appropriate potentials, both physically reasonable and computationally practical, must be developed. Unlike the all-atom models, much longer systems of thousands of base pairs must be considered; enumeration of the nonbonded interactions presents a formidable computational task.

In this work, we present a general computational model of supercoiled DNA that incorporates both elastic and electrostatic forces. Our treatment offers a computational rather than an analytical framework, such as that of Hearst and Hunt (1991), thereby permitting a study of various DNA forms without any assumptions of regularity on DNA shape (i.e., ideal interwound supercoils or toroidal forms). Our model is based on a different approach from the modified Debye-Hückel formulation of pairwise phosphate interactions recently introduced by Fenley and co-workers in short superhelical DNA (Fenley et al., 1994). Here we employ a continuum electrostatic treatment based on an experimentally derived Debye-Hückel potential (Stigter, 1977). This approach does not require modeling each phosphate explicitly and thus is practical for longer DNA systems. This new formulation can be used to study both static and dynamic processes of supercoiled DNA with algorithms developed to date (Schlick and Olson, 1992a; Schlick et al., 1994).

We show here, for a series of salt concentrations, how the configurations and energies of supercoiled DNA change dramatically depending on ionic environment. At high salt (1.0 M monovalent ions), the DNA interwound structures are very compact and locally highly bent, with the bending energy dominating over other components and the electrostatic energy playing a minor role in comparison to the bending and twisting terms. At low salt, the DNA supercoils are much more open and loose in shape, and the electrostatic components are dominant. The buckling transition between the circle and figure-8 is critically affected by the salt concentration: the large-scale configurational collapse is delayed as salt concentration decreases, with a particularly sharp increase below 0.1 M in the value of ΔLk at the transition point. The predicted changes are consistent with observations from recent cryoelectron microscopy studies and other experimental work but offer additional detailed quantitative information.

By considering electrostatic effects, we also show how the configurational regimes of DNA become more interesting than those associated with a purely elastic model. Three-lobed forms of DNA, predicted by elasticity theory to be stable equilibria (Le Bret, 1984; I. Tobias, unpublished data), describe a separate structural branch. At sufficiently long chain length and high enough superhelical density, the lobes undergo configurational transitions analogous to the circle to figure-8 conversion, leading to branched interwound forms similar to those observed in electron microscopic investigations. More generally, we find interesting trends between chain length and salt concentration. The low salt regime is particularly sensitive to chain length because repulsive interactions resist branching and interwinding. We also observe dramatic effects of salt on the dynamics of supercoiled DNA: slithering processes can be followed as well as the "collapse" of the DNA to tightly and highly bent interwound forms as salt concentration increases. At high salt, the DNA is very compact but relatively rigid, whereas at low salt the DNA becomes very open and more dynamic. These observations suggest a potential regulatory role for salt on DNA processes, not only with respect to closed circular DNA, but also for linear DNA with small looped regions. A high salt environment can condense the DNA supercoil considerably, bringing into contact segments that are far away in the linear sequence, whereas low salt conditions allow the spatially constrained double helix to undergo large configurational changes. These long-range interactions and structural variations between DNA sites may potentially play important regulatory roles in transcription and recombination.

In the next section, we present a historical perspective on previous investigations of the relationship between the structure of supercoiled DNA and salt concentration. This discussion highlights some open questions in the area. The third

section describes our DNA chain representation and energy model and develops the electrostatic treatment used in our simulations. In the fourth section, we present our results in the following areas: overall structure, buckling transitions, representative minima, energy components, lobed and branched-interwound forms, chain-length dependent studies, and DNA dynamics. We conclude with a brief summary and discussion section, which also includes additional data on simulated low-angle x-ray scattering profiles.

BACKGROUND

Although experimental information has offered valuable and well understood data on some aspects of the relationship between salt and DNA, some puzzling data still remain.

Early experimental work

One of the earliest observations of the effects of salt on superhelical DNA was that of Wang (1969), who from band sedimentation experiments noted differences in the average helical twist of a bacteriophage plasmid in the presence of different cations and counterion concentrations. The ionic strength dependence of duplex winding for all the commonly occurring counterions (Na^+, K^+, Li^+, Rb^+, Cs^+, NH_4^+, Mg^{+2}) was subsequently investigated by Anderson and Bauer (1978), who from a combination of gel electrophoresis and ultracentrifugation measurements found a linear dependence of average helical twist on the logarithm of the salt concentration. More recently, in interpreting the rates of cyclization of short linear DNAs, Taylor and Hagerman (1990) have concluded that the helical twist of DNA is independent of NaCl concentration over the range 0–162 mM. This new observation, however, may reflect the presence of 1 mM $MgCl_2$, which is necessary for the enzyme mediated ring closure in their system.

Toroidal versus interwound configurations

Early light scattering measurements of supercoiled bacteriophage ϕX174 DNA (Jolly and Campbell, 1972) concluded that at moderate salt (0.2 M NaCl) and superhelical density ($\sigma = -0.025$, see definition under Results in connection to Fig. 17) the closed chain molecule adopted a simple Y-shaped structure with evenly spaced interwound branched arms of comparable lengths. The low angle x-ray scattering profiles of superhelical DNA reported a decade later (Brady et al., 1983), however, suggested a configuration at low salt (0.01 M Na^+) consistent with a toroidal geometry. In such a form, the double helix itself wraps around the surface of a torus. However, because the relationship between the x-ray intensities and DNA shape is not one-to-one, these interpretations have remained ambiguous. Indeed, the toroidal model is incompatible with both moderate and high salt light-scattering data (Jolly and Campbell, 1972; Campbell, 1976). As we will show later, analysis of our data suggests that open interwounds at low salt, rather than toroidals, also fit the scattering data.

The existence of toroidal forms has been challenged by electron-microscopy studies that support the occurrence of branched and linear interwound supercoiled configurations (Boles et al., 1990 and references cited therein). However, because it is recognized that the micrographic procedures are rather invasive—the DNA is dyed, flattened, and dried—there remains the possibility that an artificial transition from a toroidal to an interwound form is induced by these laboratory procedures.

Meanwhile, computer simulations of DNA supercoiling using Monte Carlo and other techniques, as mentioned in the introduction, as well as analytical studies (Hunt and Hearst, 1991) based on an elastic energy function, have favored interwound over toroidal configurations. The toroidal form is consistently higher in energy. Strong support for interwound configurations has also come from knotting experiments in solution (Spengler et al., 1985); because product topology and geometry are highly sensitive to those of the original DNA substrate, the occurrence of toroidal forms in solution has appeared to be highly unlikely on the basis of observed knotting products.

Cryoelectron microscopy

Pioneering work applying less invasive cryoelectron microscopy techniques (Dubochet et al., 1988) to protein-free supercoiled DNA has provided direct evidence that the solution form of supercoiled DNA is interwound (Adrian et al., 1990; Bednar et al., 1994). Moreover, the increase of ionic strength apparently "tightens" the DNA superhelix, decreasing the diameter of the interwound double helical core in plasmids of several thousand base pairs, from 120 Å at low ionic strength to 40 Å at higher salt (10 mM Mg^{2+} or 100 mM Na^+). In shorter chains, the increase in salt concentration induces a sharp structural transition from a planar circle to a figure-8 configuration (Bednar et al., 1994), although details in this reference are not available. Clearly, the *effective diameter* of the DNA, roughly the distance of closest approach between two nonadjacent DNA segments, is a function of many factors, including internal superhelical stress, electrostatic forces, and entropic considerations. At low-salt conditions, in particular, the long-range electrostatic repulsions are expected to be important; together with entropic contributions they tend to increase the effective diameter of the DNA. Now that both mono- and divalent ions have been studied, it appears that large configurational changes are a general response of supercoiled DNA to the ionic environment. Nevertheless, there remains the possibility that the observed compaction of DNA upon addition of salt simply results from a salt-induced change in the intrinsic bending, twisting, and stretching of the double helix, as reflected in the elastic force constants deduced from the known

ionic-strength dependent variations in the persistence length (Manning, 1981).

Effective DNA diameter

Two recent studies of DNA knotting have provided more general information on the relationship between salt concentration and the effective diameter of DNA. Both Shaw and Wang and Rybenkov et al. (1993) have measured the formation of knots during random ring closure as a function of salt concentration (for both Na^+ and Mg^{2+} in the former study, and Na^+ in the latter). Both groups have found that the knotting probability p, defined as the fraction of cyclized molecules that are knotted, increases systematically with salt concentration. This is to be expected from the greater compaction of DNA at higher salt. Knotting complexity also increases with salt concentration. In the case of Mg^{2+}, the increases in knotting probabilities are more dramatic than those associated with Na^+ over the three-decade range of salt concentration that has been investigated. Very recently, these experimental trends in knotting have been simulated by lattice Monte Carlo techniques (Tesi et al., 1994).

The experimental knotting probabilities have been compared with earlier simulation-derived predictions (Klenin et al., 1988), where values for p were empirically fit to an exponential function of the form $p(d) = a\exp(-\alpha d/b)$. The parameters α and a in this expression are constants, whereas b is the assumed Kuhn statistical segment length, and d a parameter for the effective diameter of the superhelix in the simulations. The latter excluded-volume contribution is incorporated into the energy of individual chain configurations through a hard-sphere repulsive term (i.e., configurations with intersegment distances less than d are rejected from the Monte Carlo sample). The results of these comparisons—between the measured knotting probability and the effective diameters introduced to fit the data—show that as sodium-ion concentration increases from 0.01 to 2 M, d decreases from 150 to 25 Å, the lower limit corresponding approximately to the accepted geometric diameter of DNA. Significantly, at concentrations near physiological levels (0.15 M), d is roughly double the geometric diameter, a value in excellent agreement with Stigter's theoretical predictions of d for two highly charged cylinders surrounded by a Gouy double layer and an outer Debye-Hückel ionic atmosphere (Stigter, 1977), and also consistent with the packing of DNA helices in the liquid crystalline state (Livolant et al., 1989).

Shaw and Wang have further postulated that attractive interactions become important at high magnesium-salt concentrations. This is consistent with recent crystallographic observations of B-DNA (Timsit et al., 1989, 1991; Heinemann et al., 1992; Baikalov et al., 1993; Lipanov et al., 1992) that provide evidence for the close approach of double helical segments in high Mg^{2+} environments. Indeed, the crossed packing arrangements of model duplexes in these structures has been used to build atomic level representations of interwound DNA (Timsit and Moras, 1991). This attraction at counterions with higher valency is also deduced by Stigler and Dill (1993) theoretically.

Open questions

Still needed are systematic computational studies of salt effects in supercoiled DNA using realistic electrostatic potentials. The salt-dependent properties should emerge naturally from appropriate treatment of salt and other physical parameters that are introduced directly in the model (DNA length, superhelical density, etc.). Detailed quantitative energetic and structural data and dynamical analyses are needed to account for and expand on the experimental observations. A number of questions still remain unanswered: how precisely does DNA configuration change with salt concentration? How is the nonplanar writhing transition (circle to figure-8) affected by salt? Is there a critical salt environment where the collapse from loose to tight supercoils is favored? What are the characteristics of the loose forms of DNA at low salt? How does salt affect the mobility of supercoiled DNA? And how, in general, might salt play a regulatory role for biological function?

MODEL AND METHODS

B-Spline DNA representation

We represent the double-helical DNA chain by cubic B-splines, a convenient curve-fitting technique well known in numerical modeling, graphics, and industrial design (Bartels et al., 1987). To construct coordinates of the DNA chain with this model, we define a small number of control points in three dimensions. The B-spline formulas are then applied to define a closed double-helical curve, $\mathbf{r}$, for the DNA that is guided by those control points. A library of convenient sets of control points can be easily obtained by starting from the circle and minimizing the energy for various superhelical densities (see below).

Any number of curve (mesh) points can be placed on this curve and used for the interactions considered in the energy function. In the cubic B-spline formulas that we employ, each curve segment is defined locally by a linear combination of four neighboring control points, with third-order basis functions. These polynomials ensure parametric continuity of position, slope, and curvature at the junction points of the spline curve. This compact formulation provides an efficient way to model complex curves by a relatively small number of independent variables. Much larger systems than can be achieved in all-atom simulations are thus possible. A detailed mathematical description of this representation can be found in (Schlick and Olson, 1992a). Typical B-spline curves of supercoiled DNA are illustrated in the figures of that paper.

The elastic energy function

Our energy function E includes components for bending (E_B), twisting (E_T), contour length (E_L), and electrostatic interactions (E_C). The first three terms are given by the following:

$$E_B = \frac{A}{2}\oint \kappa^2(s)\,ds, \tag{1}$$

$$E_T = \frac{2\pi^2 C}{L_0}(\Delta Lk - Wr)^2, \tag{2}$$

$$E_L = K(L - L_0)^2. \tag{3}$$

In these formulas, s denotes the arc length, κ the curvature, and L the contour length of the chain. The parameters A and C are the bending and torsional rigidity constants, respectively. The twist energy follows from the assumption of an isotropic elastic rod model at equilibrium (Fuller, 1971); the twist density ω is uniform throughout the chain, and the integral term representing a quadratic deviation of the local helical twist from its intrinsic equilibrium value ω_0, $(C/2)\oint(\omega - \omega_0)^2\,ds$, can be expressed in terms of the writhing number, Wr, and the linking number, Lk. Wr is a geometric quantity that measures the shape of the curve, and Lk is a *topological invariant* describing the number of times the DNA strands intertwine around one another (White, 1989). This formulation takes advantage of the fundamental relationship proven by White (1969) that Lk is the sum of Wr and Tw (twist), where $Tw = \oint \omega\,ds$ is a measure of the total helical twist. By using E_T in the form of Eq. 2, we conveniently introduce the critical variable ΔLk, representing the imposed linking number difference as measured from a relaxed circular state Lk_0. Thus, only the curvature and the writhing number must be calculated for evaluation of the elastic terms. The computed energies are directly related to the local (i.e., base pair level) fluctuations of the chain about the assumed rodlike equilibrium rest state (see below). The isotropic rod assumption is clearly a first-order approximation and must be relaxed to study dynamical processes in detail.

The contour length term E_L is a computational device, and its contribution has a negligible effect throughout the calculation with our choice for K = 0.1 kcal/(mol Å^2). The following arc length-dependent quantities are computed by analogous discrete summations over curve points as a function of our curve parameter u:

$$L = \oint \kappa\,ds, \tag{4}$$

$$E_B = \frac{A}{2}\oint \frac{\|\mathbf{r}'(s)\times\mathbf{r}''(s)\|^2}{\|\mathbf{r}'(s)\|^6}\,ds. \tag{5}$$

We similarly compute the writhing number by the Gauss double integral (White, 1969, 1989):

$$Wr = \frac{1}{4\pi}\oint\oint \frac{[\mathbf{r}'(s_1)\times\mathbf{r}'(s_2)]\cdot[\mathbf{r}(s_1)-\mathbf{r}(s_2)]\,ds_1\,ds_2}{\|\mathbf{r}(s_1)-\mathbf{r}(s_2)\|^3}. \tag{6}$$

In all formulas above, $\mathbf{r}'$ and $\mathbf{r}''$ represent the derivatives of the curve vector $\mathbf{r}$: $d\mathbf{r}/du$ and $d^2\mathbf{r}/du^2$, respectively. The symbols $\cdot$, $\times$, and $\|\cdot\|$ denote dot products, cross products, and Euclidean vector norms, respectively. The discrete summations extend over all spline curve segments: $i = 1, 2, \cdots, N$ and over a uniform mesh for $0 \le u < 1$: $u = 0$, Δu, $2\Delta u$, $\cdots$, $(M-1)\Delta u$, where $M\Delta u = 1$. Full computational details are given in Schlick and Olson (1992a).

Elastic force constants

The elastic parameters A and C can be deduced from various experimental measurements of long-range bending and twisting (Hagerman, 1988). Although the observed values inherently reflect average sequence and ionic-medium effects, they are appropriate for a first-order, macroscopic approximation of supercoiled DNA. The bending constant A is related to the root-mean-square bending angle, $\langle\theta_b^2\rangle^{1/2}$, of a freely jointed chain through the expression $A = 2k_BTh/\langle\theta_b^2\rangle^{1/2} = ak_BT$, where k_B is the Boltzmann constant, T is the absolute temperature, h is the step-height between consecutive DNA base pairs (3.4 Å), and a is the persistence length. The value of C is similarly defined in terms of the root-mean-square twist angle, $\langle\theta_t^2\rangle^{1/2}$, because $C = k_BTh/\langle\theta_t^2\rangle^{1/2}$ and can be related by analogy to a twisting persistence length (Manning, 1988).

For this work, we choose a bending constant $A = 1.2755 \times 10^{-19}$ erg cm, corresponding to the *nonelectrostatic* contribution of the bending fluctuations to the persistence length (Manning, 1981). Although there is evidence that the persistence length increases as salt concentration decreases (e.g., a = 350 Å at 1 M and 550 Å at 0.2 M sodium), the value of a plateaus at high salt (Manning, 1981). This limiting value is generally considered to be the nonelectrostatic part of the bending constant. The change in persistence length with salt, caused by a change in DNA flexibility, is then directly accounted for in the model by the repulsive interactions in the electrostatic term. Note that this repulsion involves both the short and long-range interactions along the DNA.

Our value of the bending constant A corresponds to root-mean-square bending fluctuations $\langle\theta_t^2\rangle^{1/2} = 8.5°$ at 298 K or a persistence length a = 310 Å. We set the torsional-rigidity constant in this study so that $\rho = A/C$ = 1.5. This choice corresponds to $\langle\theta_t^2\rangle^{1/2} = 7.3°$, which corresponds to a somewhat broader range of twisting than that suggested by recent fluorescence measurements (Song et al., 1990) or that exhibited by the B-DNA crystal structures in the Nucleic Acid Database (Berman et al., 1992), where $\langle\theta_t^2\rangle^{1/2} = 5.9°$ (Olson et al., 1994).

Electrostatic energy function

To express the electrostatic energy, we formulate a Debye-Hückel potential with an effective charge per unit length. In this way, pairwise contributions along the DNA can be accumulated by considering interactions between charged DNA segments l_i. Our parameterization of this potential is based on Stigter's work (Stigter, 1977), which gives excellent agreement with experimental observation, as detailed in the previous section. Each such charged segment is centered at a mesh point of our B-spline DNA model. Thus, for N control points and M mesh points per spline segment, we consider $(NM)(NM-1)/2$ pairwise interactions between distinct (and roughly evenly spaced) charged segments along the DNA chain.

A continuum representation for a Debye-Hückel potential in a region with a linear charge density ν (charge per unit length) with charged segments l_i, l_j is given by

$$E_c = \int\int \frac{\nu^2 e^{-\beta r_{ij}}\,dl_i\,dl_j}{\epsilon r_{ij}}, \tag{7}$$

where ϵ is the dielectric constant, r_{ij} is the distance between charged segments i and j, and β is the Debye-Hückel screening parameter. At room temperature, β, in inverse Ångstrom units for monovalent counterions, is given by the relation $\beta = 0.33\sqrt{c_s}$, where c_s is the molar salt concentration.

In Stigter's formulation, the Debye-Hückel potential is obtained as a tail approximation to a Poisson-Boltzmann solution for the electrostatic interaction between two charged cylinders. Stigter uses an effective, rather than actual, charge so that the energy of Eq. 7 is written as follows:

$$E_c = B(\beta)\int\int \frac{e^{-\beta r_{ij}}\,dl_i\,dl_j}{r_{ij}}. \tag{8}$$

In this representation, the coefficient B is salt-dependent; it absorbs both the charge per unit length for the DNA and the dielectric constant of the environment. The value of B is then given by

$$B(\beta) = \left(\frac{k_BT}{2\pi}\right)\beta F(\beta), \tag{9}$$

where $F(\beta)$ is related to the effective diameter of the DNA as a function of salt:

$$F(\beta) = \exp(\beta d(\beta) - 0.7704). \tag{10}$$

The numerical value above is a constant of integration. In his derivation, Stigter sets $F(\beta)$ to the value $(2\pi\nu^2)/(\epsilon k_BT\beta)$ to result in Eq. 7 above.

In Table 1, we list for eight sodium salt concentrations in the range of 0.005 to 1.0 M the corresponding values for β, d, $F(\beta)$, and $B(\beta)$ at 300 K. We see that the Debye-Hückel coefficients $B(\beta)$ increase with increasing salt concentration. Although it is not possible to separate the effective dielectric constant from the charge per phosphate group contained within these numbers, the data are qualitatively consistent with reduction of phosphate charge by condensed counterions and a salt-dependent variation of the dielectric constant. The drop in ϵ with monovalent salt concentration, however, is significantly steeper than experimental observation (Hasted, 1973). A change of more than four orders of magnitude in $B(\beta)$ is noted over the

TABLE 1 Debye-Hückel parameters

c_s (Na^+)	β	d	$F(\beta)$	$B(\beta)$
1.0	0.330	29.5	7821.26	244.87
0.5	0.233	34.1	1321.70	29.26
0.2	0.148	44.0	305.86	4.28
0.1	0.104	56.0	159.73	1.58
0.05	0.074	74.0	108.86	0.76
0.02	0.047	112.0	86.19	0.38
0.01	0.033	157.0	82.32	0.26
0.005	0.023	223.0	84.20	0.19

Salt concentrations are given in molar units, and the Debye-Hückel parameter β is given in inverse length units ($Å^{-1}$). The effective DNA diameter d, in Ångstroms, is obtained from Stigter (1977), and the parameters $F(\beta)$ (pure numbers) and $B(\beta)$ (in units of (kcal/mol) $Å^{-1}$) are computed as discussed in the text in connection with Eq. 8.

range of salt concentrations given. In this way, appropriate effective diameters for the DNA emerge from the Debye-Hückel potential. This is clearly seen from Fig. 1, which shows a Debye-Hückel pair interaction for five salt concentrations. Note the gradual change in slope of the curves as salt concentration changes. The long-range interactions become more important as salt concentration decreases. Note also that the curves actually cross at higher energies and reverse their order. This counter-intuitive reordering of salt-dependent effects at very short contacts, however, is not expected to affect energy minimization and molecular dynamics because such high energy states are automatically excluded. More significant are the different magnitudes of the Debye-Hückel coefficients, which are critical for reproducing the correct qualitative and quantitative behavior as a function of salt. The precise value for the effective DNA diameter under given conditions will result from the *cumulative* contribution of all pairwise interactions and not from the single-pair interaction as shown here.

In practice, we compute the Debye-Hückel energy for our spline model of DNA with a discrete analog of Eq. 8:

$$E_c = B(\beta)(\Delta l)^2 \sum_{i<j} e^{-\beta r_{ij}}/r_{ij}, \tag{11}$$

where $\Delta l = (1/MN)$ is the size of a charged segment in our model. Here we set $M = 8$ and $N = 14$ following our earlier work (Schlick and Olson, 1992a). A value for the salt concentration, c_s, is assigned in each case to represent the environment, and corresponding values for B and β are determined by Table 1.

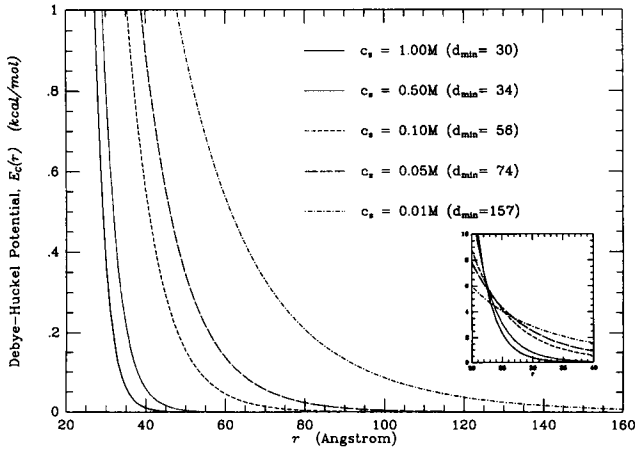

FIGURE 1 Electrostatic potentials as a function of monovalent salt concentration. For each salt concentration, the function $E_C = B(\beta)(\Delta l)^2 e^{-\beta r}/r$ is plotted over the distance, r. The salt-dependent coefficients $B(\beta)$ are given in Table 1 and discussed in the text, and the value of the charged segment length is set to $\Delta l = 30$ Å. The inset shows how the curves cross and change relative ordering at higher energy values; thus the relative magnitudes of the coefficients in the potential are crucial for correctly reproducing the DNA diameter as a function of salt.

Numerical methods

We use two methods to explore DNA structure: potential energy minimization and molecular dynamics simulations.

Energy minimization offers valuable information on favorable regions in configuration space and provides a framework for analysis of the dynamics data. The dynamical picture, including thermal fluctuations and entropic contributions, is considered separately in our dynamics simulations. The systematic energy minima and transition points that we first identify are important for interpreting configurational distributions at ambient temperatures (Ramachandran and Schlick, preprint) as well as high-energy forms (e.g., the lobed family) that may otherwise be difficult to detect in Monte Carlo or molecular dynamics simulations. High energy forms may be of interest because under certain conditions they may become more favorable (examples will be given in the next section). Essentially, the relevance of energy minimization results to DNA flexibility can be determined from the connection of minimization and dynamics results. Although the DNA motions can not be explained by simple fluctuations about one minimum state—distributions can be bimodal, trimodal, etc. (Ramachandran and Schlick, preprint)—the minima are important for characterizing certain dynamical trends, such as entropic lowering of the writhe (Schlick et al., 1994; Schlick & Olson, 1992a) and associated trends in geometric and energetic fluctuations. Significantly, Harvey and co-workers studied ensemble-averaged versus minimized-structure values for the writhing number for 600-base-pair chains and found the signal-to-noise ratio to be less than or equal to one, thereby making minimization results relevant (Sprous et al., preprint); differences are expected to increase gradually with chain length. For examples and further discussion in this connection, see Schlick et al. (1994).

The algorithm we use for minimization is the truncated Newton method, as described in Schlick and Olson (1992a). This second-derivative method uses function curvature information to converge rapidly to a minimum-energy region. The positive-definiteness of the Hessian at the minimum ensures location of a true local minimum. The independent variables in the minimization procedure are the control points of the B-spline curve, but the value of the objective function is determined from interactions involving all points along the DNA curve.

Molecular dynamics trajectories provide further information on the configuration space accessible to supercoiled DNA. A sequence of molecular configurations in time is generated by numerically integrating the classical Newtonian equations of motion repeatedly. Although Monte Carlo steps are obtained by random perturbations and thus may be designed to generate a larger ensemble of structures, molecular dynamics simulations follow *continuous* motion of the system under the influence of the force field but might sample more restricted regions of configuration space (e.g., a knotting trajectory in Schlick and Olson, 1992b). Both MD and Monte Carlo are effective configurational sampling tools. Although bending and twisting deformations are assumed to be uniformly distributed, the present simulations provide important general insights into the influence of key parameters (e.g., salt concentration) on the elastic motion of DNA and on the characteristics of the motion (e.g., global bending). An improved framework to model overdamping of the elastic modes by solvent will be reported shortly (Ramachandran and Schlick, preprint).

The algorithm we use for dynamics is the Langevin/implicit-Euler scheme ("LI"), also employed in our all-atom simulations of biomolecules, as detailed in Schlick and Olson (1992a). In the Langevin formulation, frictional and random forces are added to the systematic force (the negative gradient of the potential energy) to mimic thermal fluctuations. However, our present numerical choice of the damping constant is intended to focus on the low frequency modes and elastic parts of the motion. A physically motivated value to incorporate solvent damping into the dynamics has also been implemented (Ramachandran and Schlick, preprint). LI is particularly suitable for these studies because the high frequency modes are conveniently

absent in our macroscopic model, and larger time steps can be used than in standard explicit schemes, with overall computational gain (Schlick and Olson, 1992a; Ramachandran and Schlick, preprint). The effective time step in the B-spline model of supercoiled DNA is 100–150 picoseconds (ps), or around 10^{-10} s (Schlick et al., 1994).

The minimization and dynamics computations have been performed in double precision on a DEC alpha machine and on a Silicon Graphics Crimson/Elan minisupercomputer at New York University. A typical energy minimization on the Crimson requires several minutes to one hour, and a molecular dynamics simulation of 10,000 steps, covering a period of approximately 1.5 μs (Schlick et al., 1994) requires 8 CPU hours. Numerical and graphical analyses of polymer shape and slithering were carried out on Silicon Graphics Personal Iris and Indigo Extreme workstations at Rutgers University.

RESULTS

We first examine energy minimization results for circular DNA of 1000 base pairs with $A/C = 1.5$ as a function of ΔLk and salt. To identify detailed trends in energies and structures, we compute for five salt concentrations (c_s = 0.005, 0.05, 0.1, 0.2, and 1.0 M) minima corresponding to ΔLk in the range of 0–6 at 0.2 intervals in ΔLk. (For our purposes, the sign of ΔLk is not important, because sign reversal will simply reverse the handedness of the resulting interwounds.) In the figures below, we present complete data for three representative concentrations, because results for 0.2, 0.1, and 0.05M are similar. The summary figure at the last section includes data for all five salt values.

Small intervals of ΔLk were used to explore in detail profiles of the writhing number. In a recent work, we reported intriguing extensions of the elastic model to supercoiled DNA: higher buckling transitions (e.g., between the figure-8 and higher interwound form with two superhelical nodes) were revealed, dividing the interwound equilibrium structures into families on the basis of a sudden decrease in twist (to near-zero values) at each transition point (Schlick et al., 1994). An elastic model in combination with an attractive/repulsive Lennard Jones potential was used in those studies. However, as the results below will indicate, these potentials alone are not responsible for the trends in supercoiling; the same pattern emerges with the Debye-Hückel term. Interestingly, related transitions have been observed experimentally by Song et al. (1990) as physiological superhelical densities are approached, and also theoretically by finite-element analyses (Yang et al., 1993). Because these characteristics may be sensitive to the salt environment, we examine here similar equilibrium profiles with the new elastic and electrostatic formulation.

Overall structure

In Figs. 2-4, we present the writhing numbers and total energies of the computed DNA minima for different salt concentrations. In Figs. 6-7, we show details of the energy components. At each salt, no subtractions were made for the electrostatic energy with respect to the energy of the nicked circle at that salt environment (i.e., so that the circle will have $E_c = 0$) to allow comparison among the different salt environments. Such a subtraction would simply shift the electrostatic and, hence, the total energy at each salt regime. Many starting points for the minimization were used, such as circular forms and other minima from nearby states in each salt regime. Because the families of minima overlap, the configuration of lowest energy can be determined from the associated energy curves.

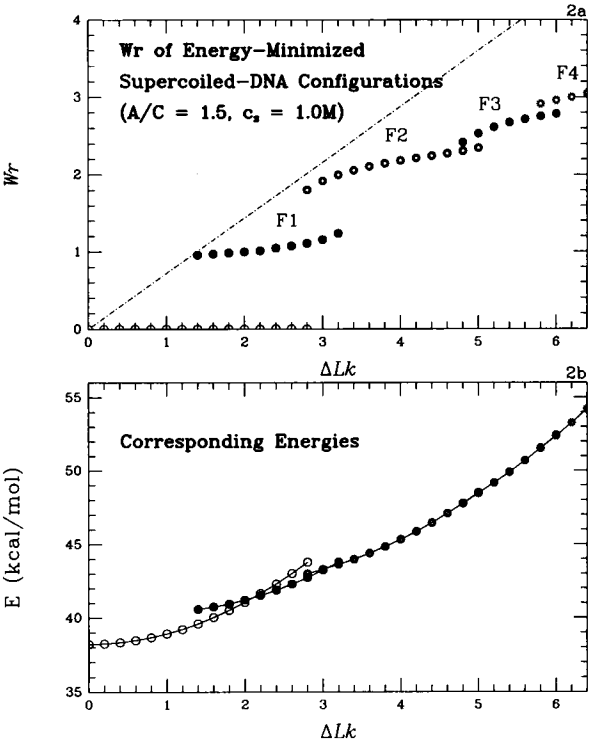

FIGURE 2 Geometry and energy for minimized supercoiled DNA of 1000 base pairs as a function of ΔLk, for $A/C = 1.5$ at 1.0 M sodium-ion concentration. (*a*) Writhing number, (*b*) total energy. The potential energy consists of elastic and electrostatic components, as detailed in the text. Each point here and in the following plots corresponds to an energy minimum, and different symbols are used to denote the different families (circle; F1 or figure-8; etc.) that emerge. The circle family is shown up to the value of ΔLk that is approximately 0.6 units (in ΔLk) beyond the value where the energies of the circle and the figure-8 are identical. See meaning of dashed line (in *a*) in the text.

We first examine the behavior at high salt (1.0 M). The effective DNA diameter is around 30 Å, the value closest to our previous model where the chosen nonbonded Lennard-Jones potential reproduced a shallow minimum at 30 Å (Schlick and Olson, 1992a). We clearly note in Fig. 2 five distinct families of DNA supercoils. (The circle with $Wr = 0$ is not labeled for consistency with our earlier work.) The first two families (at lowest ΔLk) correspond to the circle and figure-8, whereas the others are linear interwound supercoils with two or more superhelical nodes. These five families are very similar qualitatively to those identified previously, with the Lennard-Jones potential and a higher bending constant (Schlick et al., 1994). However, Wr is slightly lower here at the corresponding ΔLk with the current formulation, and also in comparison with the approximate relationship between Wr and ΔLk, $Wr = 0.72\ \Delta Lk$ (*dashed line*), estimated from ex-

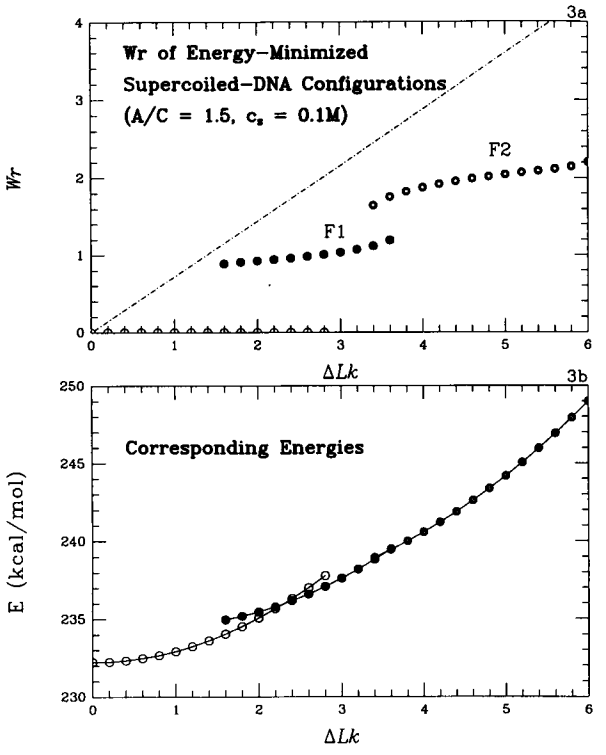

FIGURE 3 Geometry and energy for minimized supercoiled DNA of 1000 base pairs as a function of ΔLk, for $A/C = 1.5$ at 0.1 M sodium-ion concentration. (*a*) Writhing number; (*b*) total energy.

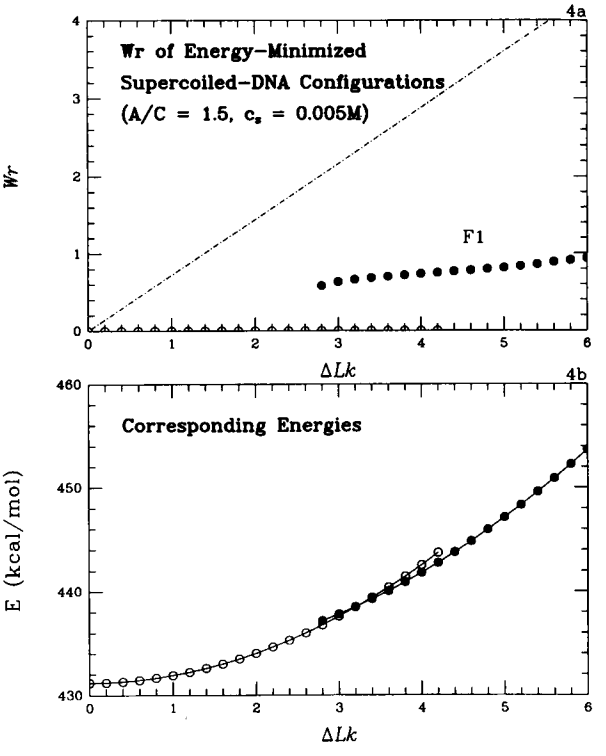

FIGURE 4 Geometry and energy for minimized supercoiled DNA of 1000 base pairs as a function of ΔLk, for $A/C = 1.5$ at 0.005 M sodium-ion concentration. (*a*) Writhing number; (*b*) total energy.

perimental analyses of long DNA supercoils (Boles et al., 1990). This is probably due to the low value of C used here. A higher value, as used in the purely elastic model (Schlick et al., 1994), would reduce $\langle\theta_t^2\rangle^{1/2}$ by 1–2° and therefore lead to equilibrium structures with higher Wr. Nonetheless, the same trends as reported here are expected, with the Wr curve shifted throughout.

Discontinuities in Wr arise from sudden changes in overall DNA shape at points where the balance of energy components is shifted (compare Figs. 2–4 with Figs. 5–7, respectively). The region between the circle and figure-8 is one such example; the associated sudden collapse (buckling) between the two stable equilibria is well understood by elasticity theory (Zajac, 1962; Le Bret, 1979; Benham, 1989). The second sudden transition corresponds to a transition from the figure-8 to an interwound form with two superhelical turns. Higher-order transitions are more subtle, and the families eventually merge into a single group at higher ΔLk. (For c_s = 1.0 M, we pursue this family up to ΔLk = 6.4). As evident from the total energy curve, the crossing of the circle and figure-8 branches is much sharper (i.e., energy differences are larger) than those associated with the other families.

As the salt concentration is decreased, we clearly note that the energy of the figure-8 is higher than that of the circle for the same ΔLk over a broader range of ΔLk (compare Figs. 2 *b*, 3 *b*, and 4 *b*). Hence, the circle is stable at higher ΔLk at low salt. Electrostatic repulsions between pairs of points along the DNA become stronger as the degree of ion screen-

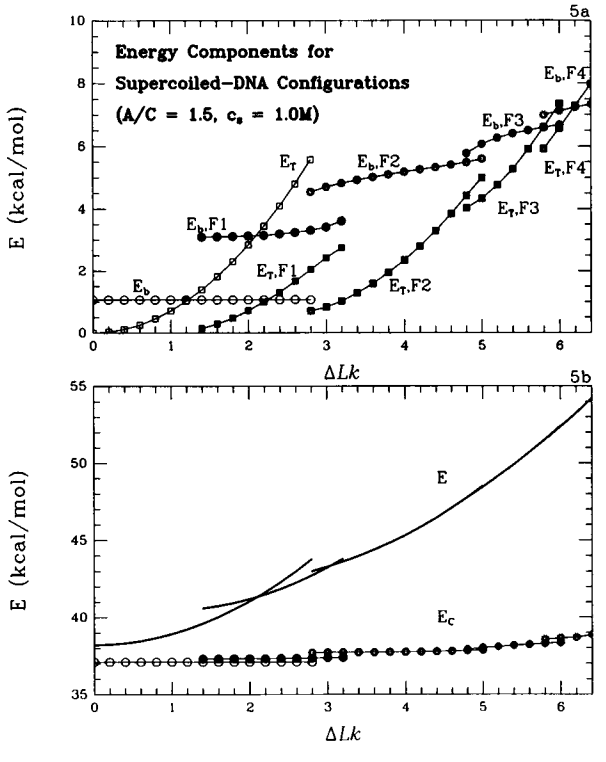

FIGURE 5 Energy components (bending, twisting, and electrostatic) for minimized supercoiled DNA forms of 1000 base pairs as a function of ΔLk, for $A/C = 1.5$ at 1.0 M sodium-ion concentration. (*a*) Elastic terms (E_B and E_T) for the families identified in Fig. 2; (*b*) Electrostatic term and total energy. The open circles and squares correspond, respectively, to E_B and E_T of the circles.

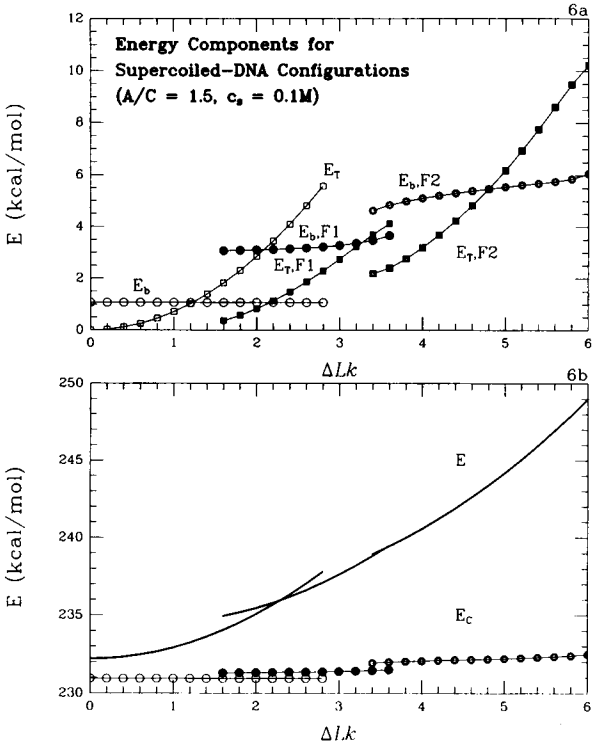

FIGURE 6 Energy components (bending, twisting, and electrostatic) for minimized supercoiled DNA forms of 1000 base pairs as a function of ΔLk, for A/C = 1.5 at 0.1 M sodium-ion concentration. (*a*) Elastic terms (E_B and E_T) for the families identified in Fig. 3; (*b*) Electrostatic term and total energy. The open circles and squares correspond, respectively, to E_B and E_T of the circles.

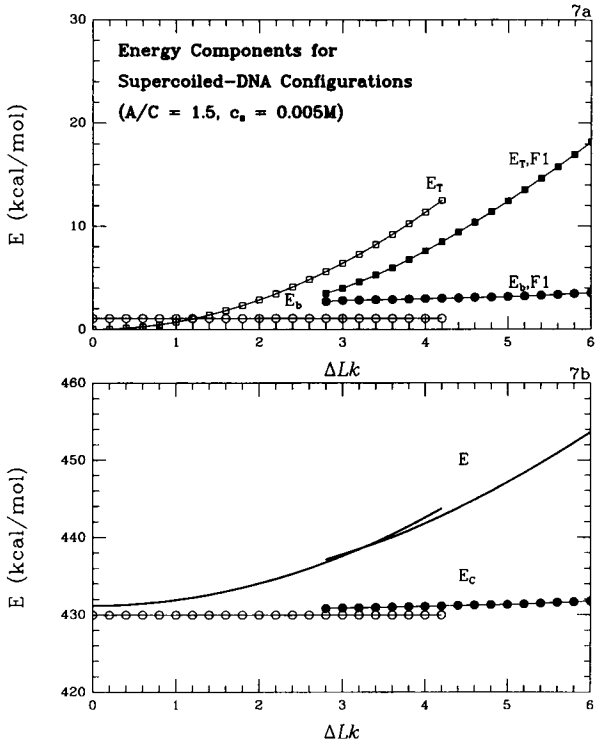

FIGURE 7 Energy components (bending, twisting, and electrostatic) for minimized supercoiled DNA forms of 1000 base pairs as a function of ΔLk, for A/C = 1.5 at 0.005 M sodium-ion concentration. (*a*) Elastic terms (E_B and E_T) for the families identified in Fig. 4; (*b*) electrostatic term and total energy. The open circles and squares correspond, respectively, to E_B and E_T of the circles

ing is reduced and the total energies are subsequently increased. There is a greater resistance to supercoiling, and the DNA forms become progressively less compact.

The writhing numbers of energy-minimized forms associated with a given ΔLk are consistently lowered as salt concentration decreases. This observation is consistent with recent Monte Carlo studies of short DNA supercoils by Fenley et al. (1994) explicitly incorporating all pairwise phosphate interactions. The combination of deterministic energy minimization and continuum electrostatic modeling in the present study, however, allows us to examine a broader range of salt concentrations, linking number differences, and chain lengths. Here not only does the figure-8 family emerge later at lower salt, but the number of distinct families of supercoils is gradually reduced, as higher writhing numbers cannot be sustained. Note, for example, in Fig. 3 that near physiological concentrations of 0.1 M salt, only three families—the circle, the figure-8, and the interwound form with two superhelical nodes—are stable up to ΔLk = 6. At extremely low salt (0.005 M), where the effective diameter of the DNA is 223 Å (Table 1), there is such great resistance to supercoiling that only the figure-8 family is found at ΔLk = 6 in the 1000 bp chain (Fig. 4). In contrast to the higher salt regimes, stable figure-8 forms are noted with writhing numbers as low as 0.6 at 0.005 M sodium. For higher salt concentrations, the figure-8 is so stable that collapsed forms with writhing numbers near unity are favored (Fig. 2). The figure-8 branch (F1) emerges at ΔLk = 1.4, 1.5, 1.6, 1.6, and 2.8 with associated values of Wr = 0.95, 0.94, 0.89, 0.81, and 0.58 at 1.0, 0.2, 0.1, 0.05, and 0.005 M salt concentrations, respectively.

Circle to figure-8 buckling

The strong effect of the salt environment on the circle to figure-8 collapse can be seen in Fig. 8. The critical ΔLk (ΔLk_c) where the energy of the circular form is equal to the energy of the figure-8 is shown for eight salt concentrations. Note that ΔLk_c = 2.1 for c_s = 1.0 M and increases to about 2.27 at c_s = 0.1 M. Beyond this point, we see a much sharper increase in ΔLk_c as salt concentration decreases. The change in critical ΔLk appears to mimic the dependence of the effective diameter on salt concentration; a similar curve is obtained if the values of d in Table 1 are plotted as a function of salt concentration. Two separate curves—one up to 0.1 M and another from 0.1 M—can be fit to both the data in Fig. 8 and that corresponding to d vs. $\log(c_s)$. Electrostatic repulsion becomes very strong at c_s = 0.1 M, and buckling from the circle to figure-8 is strongly resisted. Interestingly, this same concentration, near the physiological range, has been implicated as a point of collapse to the interwound form by Bednar et al. (1994). This idea will be discussed later as a critical salt concentration for supercoiled DNA.

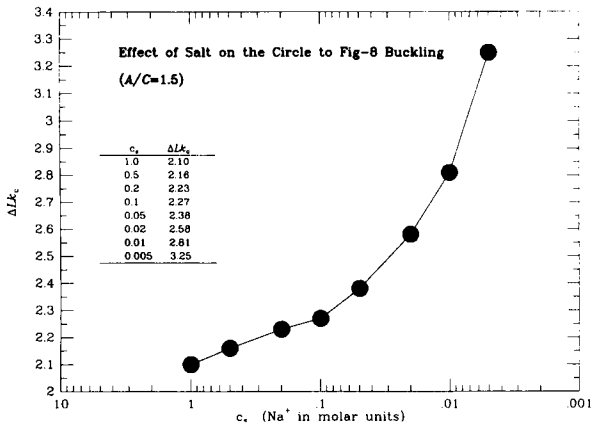

FIGURE 8 The effect of salt on the circle to figure-8 buckling for 1000 DNA base pairs, $A/C = 1.5$. The critical value of ΔLk where the energy of the circle is equal to the energy of the figure-8 form is shown against the logarithm of the salt concentration. A sharp increase is evident for salt concentrations below 0.1 M.

Representative minima

To appreciate the dramatic effect of salt on the favored supercoiled forms, we show in Fig. 9 the five minima at $\Delta Lk = 2.25$ corresponding to salt concentrations of 0.005, 0.05, 0.1, 0.2, and 1.0 M Na^+. Note that at the lowest salt the circle is the global minimum, but that a slightly imperfect circle ($Wr = 0.001$) is favored at $c_s = 0.05$ M. At $c_s = 0.1$ and 0.2 M, we find figure-8 forms, with a flatter (more collapsed) configuration at $c_s = 0.2$ M. At $c_s = 1.0$ M, the figure-8 is en route to an interwound state with two crossings.

At $\Delta Lk = 5$, the picture is even more interesting (Fig. 10). At the lowest salt, an asymmetric figure-8 is the global minimum. At $c_s = 0.05$ and 0.1 M, more compact interwound forms with $Wr = 1.9$ and 2.1, respectively, gradually emerge. Collective bending is noted as salt is further increased, so that at $c_s = 1.0$ M a globally bowed supercoil is observed, with end loops directed toward each other and the two central interwound segments in close contact. Repulsive interactions are effectively screened under these conditions, so that sequentially distant residues can approach one another. Significantly, in no case do any parts of the DNA come as close as the effective diameter implied in the Debye-Hückel parameters used in the calculations. The mean distance between contacted chain segments $\langle D_{\Delta Lk=5} \rangle$ in the interwound minima at $\Delta Lk = 5$ is proportional to d, closely fitting the expression $\langle D_{\Delta Lk=5} \rangle = 11.26 + 1.03d$ Å.

Energy components

Turning now to the analysis of energy components as a function of salt, we examine the patterns in Figs. 5–7. These plots detail the bending, twisting, electrostatic, and total energies associated with each of the supercoils at the specified salt concentrations. The electrostatic energy increases as salt concentration decreases by straightforward calculation of the Debye-Hückel potential (i.e., without any subtraction with respect to the nicked circle at each salt). The values of E_B in Figs. 5–7 rise with ΔLk because the chain evolves into more compact structures. The twisting contributions (E_T), in contrast, tend to rise within individual supercoiled families and then drop suddenly at points of sudden configurational collapse (see below). The electrostatic repulsions increase as more DNA segments come into closer contact. However, whereas at high salt, only nearby repulsions contribute significantly, at low salt the number of long-range repulsions among unscreened DNA segments increase the electrostatic energy significantly.

The bending energy is a minimum in the circle. It then increases abruptly as the figure-8 branch is reached, with the increase accompanied by a sharp drop in E_T. This drop in E_T is sharpest for the higher salt, and it becomes progressively less so as salt concentration is decreased. Because the different families of supercoils begin at a low-twist energy (Schlick et al., 1994), similar qualitative trends (rise in E_B, drop in E_T) are noted for the higher order transitions between families, with sharpness decreasing as salt concentration increases.

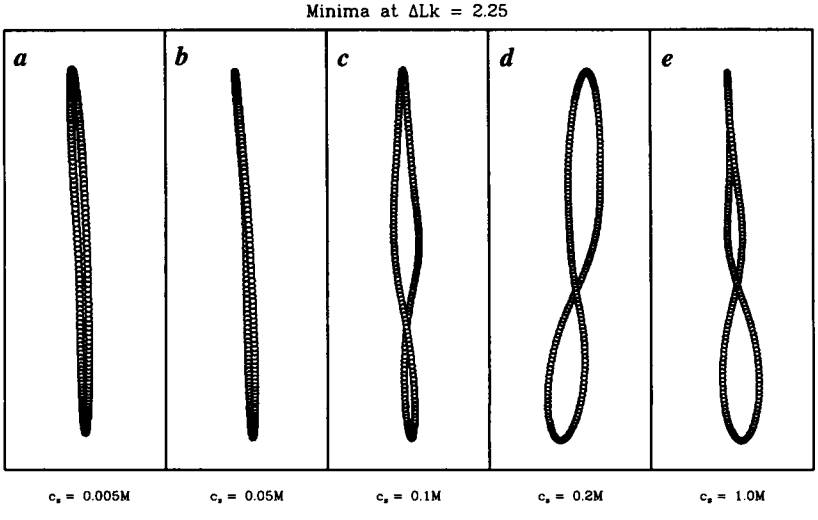

FIGURE 9 Energy minima for supercoiled DNA of 1000 base pairs, $A/C = 1.5$, at $\Delta Lk = 2.25$ as a function of salt concentration: (*a*) $c_s = 0.005$ M, with $Wr = 1.03$, $E_B = 3.16$, $E_T = 1.06$, $E_C = 37.33$ kcal/mol. (*b*) $c_s = 0.05$ M, with $Wr = 0.968$, $E_B = 3.13$, $E_T = 1.17$, $E_C = 166.1$ kcal/mol. (*c*) $c_s = 0.1$ M, with $Wr = 0.948$, $E_B = 3.12$, $E_T = 1.21$, $E_C = 231.3$ kcal/mol. (*d*) $c_s = 0.2$ M, with $Wr = 0.001$, $E_B = 1.07$, $E_T = 3.56$, $E_C = 291.4$ kcal/mol. (*e*) $c_s = 1.0$ M, with $Wr = 0.000$, $E_B = 1.07$, $E_T = 3.60$, $E_C = 430.0$ kcal/mol.

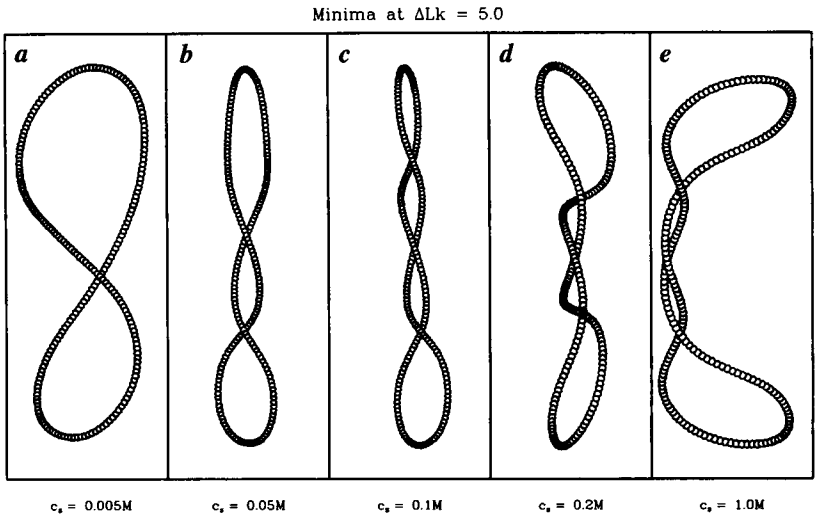

FIGURE 10 Energy minima for supercoiled DNA of 1000 base pairs, $A/C = 1.5$, at $\Delta Lk = 5.0$ as a function of salt concentration: (*a*) $c_s = 0.005$ M, with $Wr = 2.58$, $E_B = 6.15$, $E_T = 4.18$, $E_C = 38.1$ kcal/mol. (*b*) $c_s = 0.05$ M, with $Wr = 2.16$, $E_B = 5.56$, $E_T = 5.75$, $E_C = 166.9$ kcal/mol. (*c*) $c_s = 0.1$ M, with $Wr = 2.05$, $E_B = 5.55$, $E_T = 6.19$, $E_C = 232.2$ kcal/mol. (*d*) $c_s = 0.2$ M, with $Wr = 1.89$, $E_B = 5.45$, $E_T = 6.86$, $E_C = 292.8$ kcal/mol. (*e*) $c_s = 1.0$ M, with $Wr = 0.82$, $E_B = 3.19$, $E_T = 12.41$, $E_C = 431.3$ kcal/mol.

Lobed family and branched interwound structures

The consideration of both the elastic and electrostatic energies reveals a wider spectrum of favorable configurational states. By performing minimizations at various values of ΔLk and salt concentration from a three-lobed unknotted supercoil—obtained by altering several control points of a DNA trefoil knot (Schlick and Olson, 1992b)—we find an entirely new family of three-lobed DNA shapes that form branched interwound structures at higher salt and longer chain length (see below). Such branched forms are the prevalent form of supercoiled DNA for longer chains (e.g., 3500 base pairs and more) and are commonly observed in electron micrographs (Boles et al., 1990). A stronger resistance to branching and interwinding at low salt produces very open three-lobed (branched) forms in comparison with high salt.

In Figs. 11-13, we show the lobed families for salt concentrations of 1.0, 0.1, and 0.005 M sodium corresponding

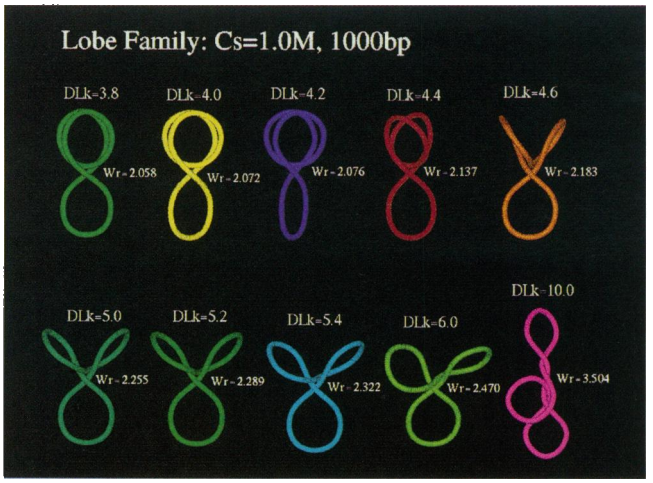

FIGURE 11 The lobed family for 1000 base pairs, $A/C = 1.5$, and $c_s = 1.0$ M. Forms are shown from the initial value of ΔLk, ΔLk_L, where a lobed form is a stable equilibria.

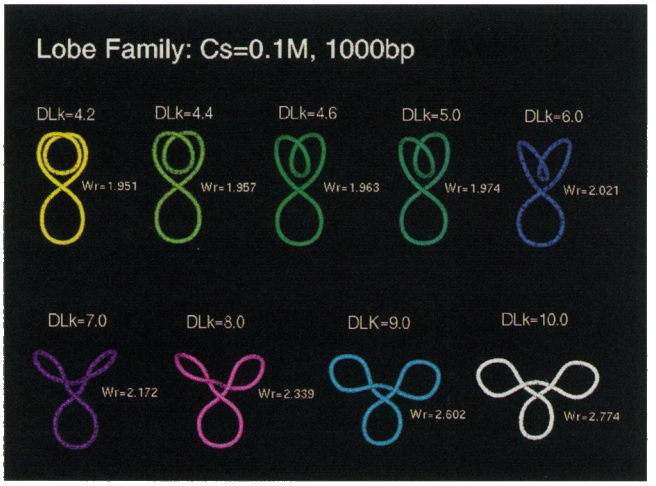

FIGURE 12 The lobed family for 1000 base pairs, $A/C = 1.5$, and $c_s = 0.1$ M.

to ΔLk between the two values ΔLk_L (the lowest value where a lobed form is stable) and 10. The value of ΔLk_L and the geometrical details of the associated lobed configurations are highly salt-dependent. At higher salt environments, the first stable lobed state that emerges resembles a figure-8 in shape with an additional intertwined loop. It has approximately two superhelical turns. At low salt, a very open, globally-bent triangular form is obtained.

Fig. 14 displays at eight salt environments those lobed forms at the beginning of the family, ΔLk_L. Note the very tight loops at high salt and the loose, open configurations at low salt. At $c_s = 1.0$, 0.1, and 0.005 M, $\Delta Lk_L = 3.8$, 4.2, and 8.4, respectively. For each of the lobed families (Figs. 11–13), basically similar patterns are noted as ΔLk increases beyond ΔLk_L. The intertwined loop in one part of the figure-8 gradually changes orientation until two distinct lobes emerge. These lobes gradually move apart from one another at roughly perpendicular orientations to form a central region separating the three lobes. As ΔLk increases further, the three lobes become more planar and open. At high salt, further

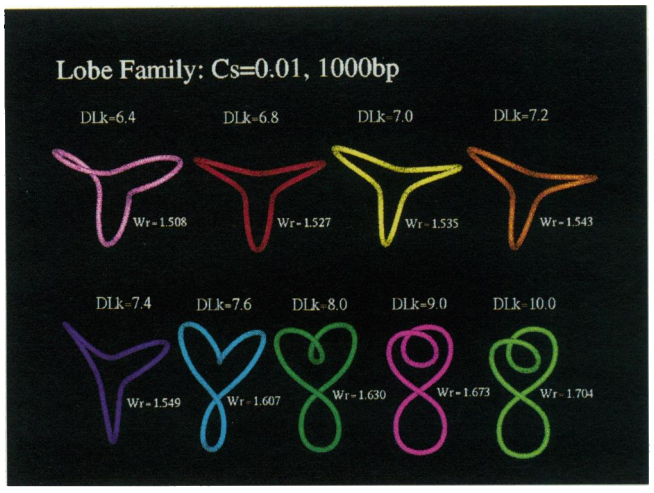

FIGURE 13 The lobed family for 1000 base pairs, $A/C = 1.5$, and $c_s = 0.01$ M.

FIGURE 15 Members of the lobed family for 1000 base pairs, $A/C = 1.5$, $\Delta Lk = 10$, for different salt concentrations. Note the very wide range of forms, from bent triangular at low salt to branched interwound at high salt.

FIGURE 14 The first member of the lobed family for 1000 base pairs, $A/C = 1.5$, for different salt concentrations. The form shown at each salt value corresponds to ΔLk_L, the smallest ΔLk where a lobed form is a stable energy minimum.

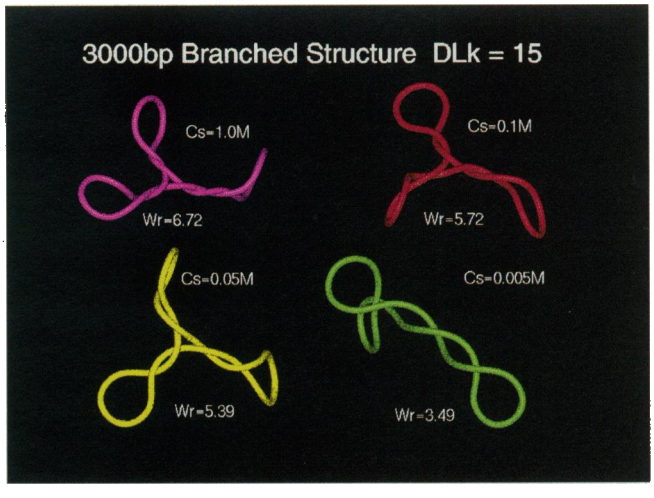

FIGURE 16 Branched-interwound supercoils for 3000 base pairs, $A/C = 1.5$, $\Delta Lk = 15$, for different salt concentrations. Note the very tight and bent interwound forms at high salt and open and loose form at low salt.

interwinding begins to separate two of the lobes to differentiate a "stem" region, which then supercoils to produce an interwound form. A corresponding transition between planar three-lobed and branched interwound minima is also found for the simple elastic model (G.-H. Liu, W. K. Olson, and T. Schlick, preprint).

The change in Wr with increase in ΔLk within the lobed family is much smaller than that shown by simple interwound structures (Figs. 2–4) of the same size (1000 base pairs). The much higher bending energies associated with the three-lobed forms, in comparison with the straight interwound configurations (see below), explain this behavior.

To examine how increasing ΔLk would affect the lobe geometry, we show in Fig. 15 the members of the lobed family at each salt concentration corresponding to $\Delta Lk = 10$ (clearly, this corresponds to a value higher than typical physiological densities). Note the wide spectrum of shapes, from open triangular at $c_s = 0.005$ M ($Wr = 1.4$) to branched interwound at $c_s = 1.0$ M ($Wr = 4.1$). Only for longer chain lengths do branched interwound forms emerge at very low salt. In Fig. 16, four branched interwound minima for chains of 3000 base pairs with $\Delta Lk = 15$ are shown for $c_s = 0.005$, 0.05, 0.1, and 1.0 M salt. Note the very tight and bent branched interwound minima at high salt, which gradually open as salt decreases and form a longer interwound stem with two short lobes at the extreme low salt end. For these longer DNA, differences in the bending and electrostatic terms become smaller between the branched and unbranched forms (in comparison with the 1000 base pair chain) so that branched forms are favored. Entropic effects and thermal fluctuations also make the branched forms more favorable at longer chain lengths (Vologodskii et al., 1992).

Table 2 compares the energy components and writhing numbers for the 1000 base-pair lobed and interwound

TABLE 2 Energetics of lobed versus interwound forms for 1000 base pairs: $A/C = 1.5$

Parameters	Form	E_B	E_T	E_C	E	Wr
c_s = 1.0 M						
$\Delta Lk_L = 3.8$	Int.	5.107	1.942	37.747	44.835	2.15
	Lobe	8.569	2.158	38.405	49.172	2.06
$\Delta Lk = 6.0$	Int.	7.125	6.573	38.634	52.372	2.96
	Lobe	9.083	8.857	39.558	57.540	2.47
c_s = 0.2 M						
$\Delta Lk_L = 4.2$	Int.	5.274	3.301	166.780	175.540	2.05
	Lobe	8.716	3.411	167.594	179.908	2.01
$\Delta Lk = 6.0$	Int.	6.404	9.091	167.285	182.966	2.42
	Lobe	8.729	10.709	168.124	187.750	2.12
c_s = 0.1 M						
$\Delta Lk_L = 4.2$	Int.	5.216	3.687	232.099	241.213	1.92
	Lobe	8.592	3.596	232.971	245.373	1.95
$\Delta Lk = 6.0$	Int.	6.068	10.215	232.501	248.997	2.21
	Lobe	8.669	11.254	233.223	253.361	2.02
c_s = 0.05 M						
$\Delta Lk_L = 4.6$	Int.	5.267	5.461	292.733	303.675	1.83
	Lobe	8.414	5.299	293.633	307.561	1.87
$\Delta Lk = 6.0$	Int.	5.817	11.298	293.055	310.383	2.01
	Lobe	8.552	11.811	293.754	314.333	1.92
c_s = 0.005 M						
$\Delta Lk_L = 8.4$	Int.	4.864	35.888	433.385	474.307	1.30
	Lobe	7.288	34.912	434.149	476.520	1.39

Salt concentrations are given in molar units, and energies (bending, twisting, electrostatic, and total) are given in kcal/mol. For each salt concentration except the last one, two sets of interwound (Int.) and lobed (Lobe) forms are described: at ΔLk_L, a salt-dependent value where a lobed family is first identified as a minimum, and at $\Delta Lk = 6$.

minima at ΔLk_L and $\Delta Lk = 6$ for different salt concentrations. For $c_s = 0.005$ M, $\Delta Lk_L = 8.4$, so we only compare the lobed and interwound configurations at this value. It is evident that the major difference in energy between the three-lobed and interwound forms arises from a higher bending energy for the lobed families. At ΔLk_L, the bending energy difference ΔE_B is greater by 3 kcal/mol at high salt but is lowered as salt concentration decreases. At $\Delta Lk = 6$, ΔE_B is approximately 2 kcal/mol at 1.0 M salt, and is increased as salt concentration decreases. The twisting energy differences are quite small at ΔLk_L, but larger at $\Delta Lk = 6$, especially at high salt. This can be explained by the slower increase of Wr with ΔLk in the lobes in comparison to the interwound forms at high salt, as noted above. The increasing difference in their values gives rise to the increase in E_T.

In contrast to the elastic terms, the electrostatic energy differences are overall quite small (roughly less than 1 kcal/mol) for all ΔLk and salt concentrations. Overall, these observations suggest that the lobed family is some part of the population of superhelical forms, especially at low salt. This is verified by the dynamical simulations (see below).

Chain length and salt

The previous section detailed the effects of DNA length on the types of favorable equilibria (branched vs. unbranched interwound states) and the effects of salt on branching tendencies (e.g., stronger initial resistance to branching at low salt, but greater likelihood of branched forms once energetically stable). To study these trends more systematically and to gain further insight into the relative contributions of the elastic and electrostatic components, we performed several minimizations for shorter DNA chains of 875, 750, and 625 base pairs. These lengths were chosen because the mesh size of the B-spline model could be changed by integral values to produce the same size of charged linear segments as considered in the 1000-base-pair simulations. We fix the value of σ, the superhelical density ($\sigma = \Delta Lk/Lk_0$), in these studies rather than ΔLk to impose the same relative superhelical strain. For simplicity, we take ω_0 to be independent of salt in computing Lk_0 from the expression $Lk_0 = Tw_0 = \frac{1}{2} \oint \omega_0 \, ds$. The error in this approximation is negligible considering the small measured variation in average helical twist with salt concentration together with the short chain lengths treated here.

Fig. 17 shows the energy components and writhing numbers as a function of DNA length for the two cases $\sigma = 0.05$ and $\sigma = 0.03$ at two salt concentrations (0.05 and 1.0 M). The

FIGURE 17 Energetic and geometric trends for different DNA lengths at two extreme salt environments. Shown here are the writhing numbers, bending, twisting, electrostatic, and total energies corresponding to equilibria forms of DNA (625, 750, 875, and 1000 base pairs) at salt concentrations of 1.0 and 0.05 M for two superhelical densities. (*A*) $\sigma = 0.05$ and (*B*) $\sigma = 0.03$. For $\sigma = 0.05$, $\Delta Lk = 5$, 4.375, 3.75, and 3.125 for 1000, 875, 750, and 625 base pairs, respectively. For $\sigma = 0.03$, the corresponding ΔLk values are: 3, 2.625, 2.25, and 1.875. The elastic and electrostatic energy functions are used as described in the text, with $A/C = 1.5$. Energies are given in kcal/mol and are normalized per 100 base pairs. For $\sigma = 0.05$, two configurational families are encountered: F1 and F2 (see Figs. 2 and 3), so only connections within the same family are displayed.

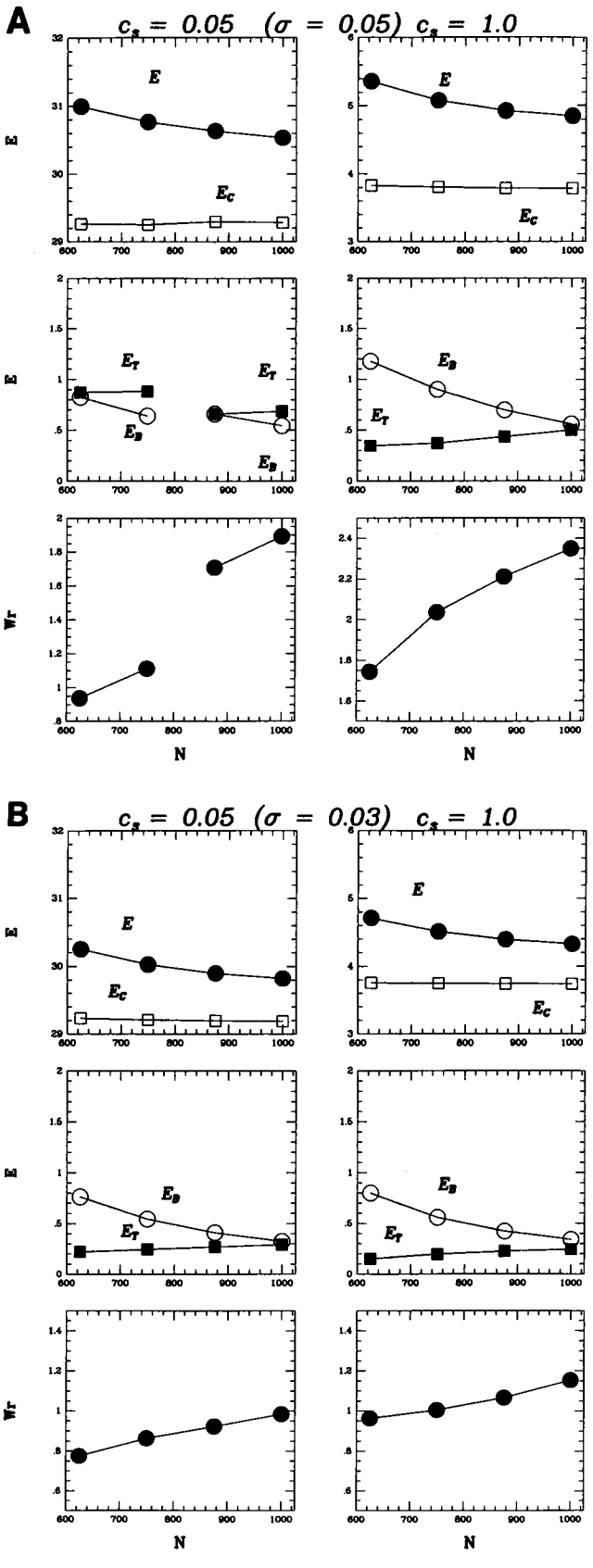

energies are normalized (i.e., per 100 base pairs). The electrostatic energy increases with length as expected, because the number of repulsive interactions increases, and thus the normalized value remains similar for all chain lengths. The bending energy is higher for shorter chains and decreases as chain length increases *within the same configurational family*. Note that for $\sigma = 0.05$ there are two such families at low salt: the figure-8 (F1) and the interwound form with approximately two superhelical nodes (F2). The twisting energy, on the other hand, increases slightly with DNA length for each family. (The drop in E_T noted at $\sigma = 0.05$ for 875 base pairs at low salt is associated with the emergence of the F2 family). The total normalized energy decreases slightly with length because of the bending energy decreases.

We also note from these plots that the equilibrium values of Wr are lower for shorter chains (with σ and salt fixed). This can be attributed to the higher bending energies that make supercoiling more difficult for shorter DNA. However, even though Wr is lower, ΔLk is also lower for shorter chains with the same σ, so E_T is lower for shorter plasmids.

These trends in the elastic energies as a function of chain length and salt also affect the buckling transition from the circle to the figure-8. We obtain essentially the same trend as that displayed in Fig. 8—delayed buckling as salt concentration decreases—but for shorter chains the delay is sharper at low salt. These tendencies have also been noted by Fenley et al. (1994), although the precise locations of the configurational transitions are shifted to lower ΔLk when the electrostatic energy is computed for all pairs of phosphate atoms. Fig. 18 presents the critical superhelical density, σ_c, where the energies of the circle and figure-8 families are identical for the four DNA lengths examined. A systematic shift in σ_c emerges as length decreases for each concentration. This can be explained by the higher bending energy of the interwound forms in shorter duplexes (i.e., larger energy

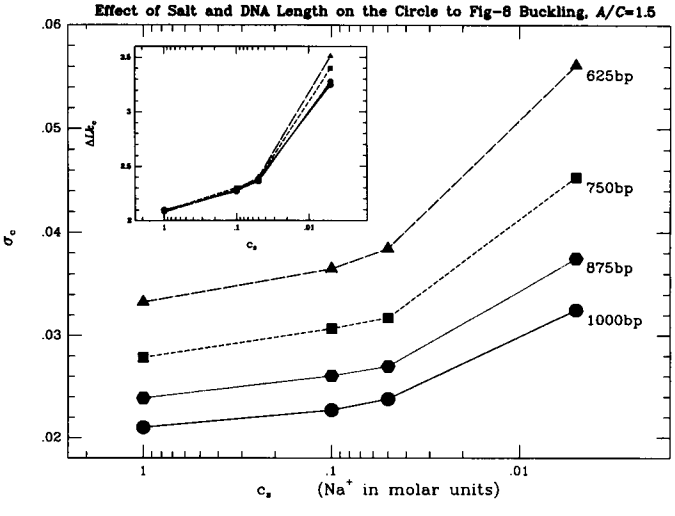

FIGURE 18 Buckling transition for different DNA lengths as a function of salt, $A/C = 1.5$. Critical superhelical densities where the energies of the circle and the figure-8 are equal are shown for 625, 750, 875, and 1000 base pairs. The inset shows the critical ΔLk instead of σ and reveals the particularly sharp delay of buckling at low salt for shorter chains.

difference compared to the circle) and, therefore, a greater resistance to buckling. The shift is also larger at low salt, again reflecting the choice of the effective diameter d in the electrostatic potential. The sharper increase at low salt can be seen as well from the inset of Fig. 18, displaying ΔLk_c rather than σ_c.

Molecular dynamics simulations

To obtain further insight into the characteristic motions of supercoiled DNA as a function of salt, we have simulated the dynamics of a 1000-base-pair DNA at three salt environments. Representative concentrations of 0.005, 0.1, and 1.0 M salt were used in three trajectories covering approximately 1 μs (Schlick et al., 1994) at room temperature. All trajectories were started from the equilibrium configurations corresponding to $\Delta Lk = 5$, with elastic parameters $A/C = 1.5$ and $\Delta Lk = 5$ fixed throughout. The computed results are thus expected to reveal average fluctuations about these minima dictated by the systematic force as a function of salt. Because damping effects are not presently incorporated (except indirectly through the experimentally measured elastic constants), only motions of the dominant elastic modes are expected. Table 3 summarizes various statistical quantities obtained from these dynamics trajectories: mean values, variances, and ranges for the writhing numbers and the bending, twisting, electrostatic, elastic (bending plus twisting), and total energies.

TABLE 3 Statistical quantities averaged from molecular dynamics trajectories

Property	c_s = 0.005 M	c_s = 0.1 M	c_s = 1.0 M
W_r, mean	0.77	2.01	2.56
W_r, var.	6.58×10^{-2}	1.85×10^{-1}	1.31×10^{-1}
W_r, range	0.54–0.96	1.53–2.39	2.26–2.89
	(0.42)	(0.85)	(0.63)
E_B, mean	3.41	5.98	6.31
E_B, var.	0.287	0.616	0.370
E_B, range	3.00–4.77	4.76–7.42	5.67–7.50
	(1.77)	(2.66)	(1.83)
E_T, mean	12.72	6.37	4.25
E_T, var.	0.397	0.792	0.455
E_T, range	11.60–14.17	4.86–8.54	3.16–5.35
	(2.57)	(3.69)	(2.19)
E_C, mean	431.50	232.46	38.19
E_C, var.	0.381	0.353	0.320
E_C, range	431.0–434.5	232.0–235.4	37.82–40.58
	(3.5, 0.8%)	(3.4, 1.4%)	(2.76, 6.8%)
$E_B + E_T$, mean	16.13	12.35	10.57
$E_B + E_T$, var.	0.459	0.569	0.326
$E_B + E_T$, range	15.49–17.87	11.51–14.41	10.15–12.22
	(2.38, 13%)	(2.9, 20%)	(2.1, 17%)
E, mean	447.79	245.02	48.79
E, var.	0.693	0.690	0.533
E, range	447.11–451.34	244.18–247.56	48.45–51.79
	(4.23, 0.9%)	(3.38, 1.4%)	(3.34, 6.5%)

Entries are averaged from three trajectories at room temperature for 1000 base-pair DNA, with $A/C = 1.5$ and $\Delta Lk = 5$. Trajectories were started from the equilibrium configurations at each salt concentration. Total simulation time was 1 μs. Energies are measured in kcal/mol, and percentages are given for some energy ranges to highlight the differences.

The following interesting trend emerges from the data. In overall flexibility, the DNA is most dynamic at the 0.1 M salt environment, followed by the 0.005 M and then the 1.0 M salt concentrations. This is clearly seen from the overall hierarchy in magnitudes of the variances and ranges for the writhing numbers and energy components. The greatest differences are evident for Wr, E_B, E_T, and $E_B + E_T$. For example, the range of Wr fluctuations for $c_s = 0.1$ M is 0.85 (roughly 36%) vs. 0.63 (22%) and 0.42 (43%) for $c_s = 1.0$ and 0.005 M, respectively. The trends do not completely follow the expected effects of the electrostatic potential as the salt is lowered. The greater range of shapes at 0.1 M vs. 0.005 M salt is unexpected on the basis of electrostatic arguments, but consistent with the presence of two stable minima at the higher salt concentration (an interwound form with $Wr = 2.05$ and a lobed configuration with $Wr = 1.97$). The simulation at 0.1 M salt samples both minima, whereas only the interwound form prevails at 0.05 M. The variances and fluctuations of E_B and E_T at $c_s = 0.1$ M also reflect the presence of two minima. The variances are nearly double the quantities associated with $c_s = 1.0$ and 0.005 M, and the fluctuation ranges are roughly 50–75% larger. These fluctuations might change with the explicit incorporation of solvent damping, but the hierarchy noted here is likely to be preserved.

As expected, the mean values of Wr and E_B increase with salt, whereas the mean E_T, E_C, $E_B + E_T$, and the total potential energy decrease with salt. The electrostatic energy decreases as salt concentration increases, but both the overall variance (about 0.35) and the range of E_C fluctuations (about 3 kcal/mol) are similar for all three salt concentrations. The magnitudes of the variances and fluctuation ranges of the total potential energy are similar for all three sets.

To explore how a changed salt environment might affect these patterns, we also simulated the dynamics of DNA where the salt concentration was changed during the course of the simulation. This hypothetical protocol, although clearly leading to dramatic rather than gradual changes in DNA shape, might provide some insight into the possible regulatory role that salt might have on DNA. Statistical properties from dynamics of equilibrated systems are given separately in Table 3. Although details are not known, the salt concentration is likely to change in the realistic cellular environment. Snapshots for a 1000-base-pair DNA plasmid covering approximately 1 μs, started from a circular configuration, are shown in Fig. 19. The salt concentration was set to 1.0 M at the onset and midpoint of the simulation and changed to 0.01 M at iterations 1000 and 4000, for 2000 steps after each resetting. (Each time step corresponds to 150 ps.)

We note from the figure how the tightly interwound forms at high salt open as the salt is decreased and reveal a larger range of possible configurations. We also see an apparently slower rate of end-over-end tumbling of the low salt DNA. Forms resembling the lobes detected by energy minimization are evident in several snapshots at 0.01 M salt. These loosely coiled branched forms appear to be associated with transitions from the high to medium salt environments.

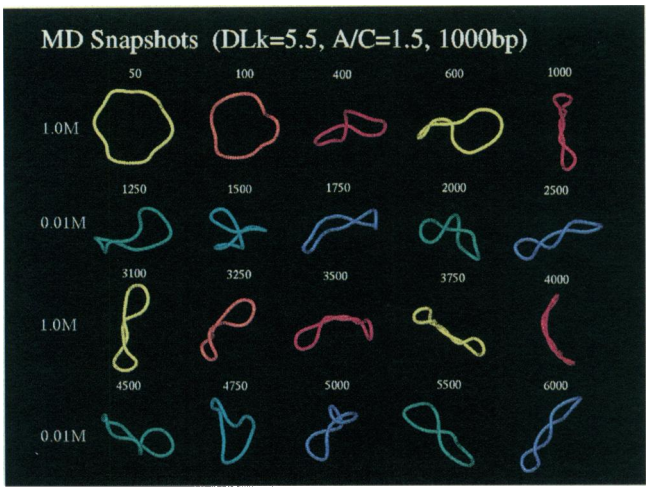

FIGURE 19 Molecular dynamics snapshots from a simulation at alternating salt concentrations. The trajectory was performed at room temperature for 1000 base pairs, $A/C = 1.5$, and $\Delta Lk = 5.5$. The salt concentration was set to 1.0 M during iterations 0–999, 3000–3999, and to 0.01 M at iterations 1000–2999, and 4000–6000.

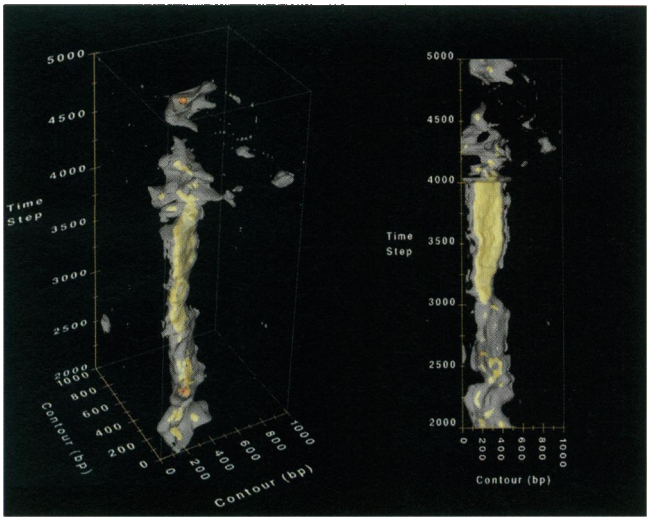

FIGURE 21 Pairwise contributions to the writhing number of supercoiled DNA configurations sampled by molecular dynamics. The color-coding depicts the pairs of contour points (s_1 and s_2) making the largest contributions Wr_{s_1,s_2} to the writhing number of each configuration sampled along the dynamics trajectory described in Fig. 19. Pairwise interactions of magnitude 0.005 or more lie (Eq. 6) within the yellow regions, and contacts of magnitude 0.001 or more within the larger transparent white volumes. Note the different character of the interactions at high versus low salt (steps 3000–4000 versus steps 2000–3000 and 4000–5000). Refer to the text for additional details.

The different behavior of the chain at low and high salt is further apparent from the principal moments I_1, I_2, and I_3 of the radius of gyration, reported in Fig. 20 in terms of the moment ratios, $R_1 = (I_2 + I_3)/I_1$ and $R_2 = (I_2 - I_3)/I_1$, over the course of the simulation. The sharp increase in R_1 (to values greater than unity) at each drop in salt concentration reflects the sudden overall opening of the DNA with increased strength of electrostatic interactions. This expanded structure subsequently relaxes to a loose interwound form with approximate cylindrical symmetry (i.e., $R_2 \approx 0$). The asymmetry ratio, R_2, is somewhat greater at high salt, mirroring the collective bending and twisting of the chain as a whole.

Fig. 21 illustrates another aspect of the chain dynamics. Here we plot over part of the simulation the contributions Wr_{s_1,s_2} to the writhing number from all pairs of contour points

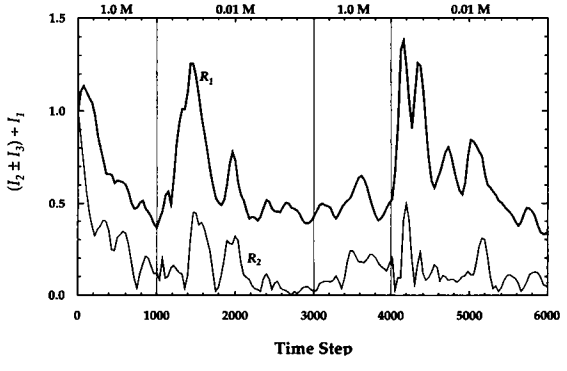

FIGURE 20 Ratios of principal moments of the radius of gyration as a function of iteration. The two moment ratios, $R_1 = (I_2 + I_3)/I_1$ and $R_2 = (I_2 - I_3)/I_1$, are rough descriptors of overall molecular shape over the course of the dynamics simulation outlined in Fig. 19. The principal moments, I_1, I_2, I_3, are computed from the parametric B-spline curve of the DNA, as described previously (Schlick and Olson, 1992a, Schlick et al., 1994).

(s_1 and s_2) along the double helical axis (see Eq. 6). These data, which show the parts of the chain in intimate contact at designated times along the trajectory, are represented in terms of a three-dimensional color-coded volume (*left*) and its projection (*right*) in the chain contour/time-step plane. The largest pairwise contributions, where the magnitude of Wr_{s_1,s_2} is 0.005 or more, are highlighted in yellow. These regions, typically found in the central contact zone of an interwound supercoil, are predominant at high salt. Moreover, the regular dimensions of the highlighted domain point to a fairly rigid contact zone of 200–250 bp in the high salt environment (steps 3000–4000). Essentially the same pairs of points remain in close contact at 1.0 M salt. By contrast, there are very few long-range contacts in the DNA supercoil at 0.01 M salt (steps 2000–3000 and 4000–5000), with only fleeting associations of sequentially distant segments. Some of the low salt configurations entail three or more isolated points of contact, such as found in a lobed structure, whereas others include more closely spaced associations typical of a loose interwound supercoil. Parts of the DNA also appear to "slither" rapidly past one another at low salt. The irregular shapes of the yellow volumes in this regime are indicative of chain movement, because different parts of the DNA comprise the close contacts over a short time interval. The summation of contributions to *Wr* from contour points within the transparent white regions (where $|Wr_{s_1,s_2}|$ is greater than 0.001) account for essentially 100% of the writhing number of any configuration. Thus, the contour levels also reveal the reduced magnitude of the writhing number with decrease of salt. The virtual absence of any contributions to *Wr* at some

time steps (e.g., 4750) shows that the low salt chain also opens occasionally to nearly circular forms.

SUMMARY AND DISCUSSION

It has long been recognized that electrostatic interactions play an important role in determining DNA structure and the interactions of DNA with surrounding molecules. The salt concentration in the natural cellular environment of the DNA affects these properties and processes profoundly, because the degree of phosphate shielding by positive ions determines the nature of both the short-range and long-range contacts along the DNA. At high salt, the negative charges along the DNA backbone are effectively screened, permitting closer contacts, whereas at low salt the repulsive forces keep DNA segments apart. These factors are particularly important for supercoiled DNA, where the enthalpic (elastic and electrostatic components) and entropic forces compete to determine the favorable geometries of long-range contacts at a given environment.

Only recently have conclusive data been obtained for the effective diameter of DNA as a function of salt (Bednar et al., 1994). Significantly, at physiological salt concentrations (e.g., 0.15 M sodium), the diameter of a virtual cylinder around which superhelical DNA can be imagined to wind is already double (50 Å) the geometric value. This effective diameter reaches triple the geometric value as the salt concentration is decreased by an order of magnitude (0.01 M). Although it has been traditional to use simple hard-sphere potentials in computational and theoretical models of DNA supercoiling, it is clear that only more detailed electrostatic treatments can capture accurately the complex effects of salt on the geometric characteristics, energetics, and dynamics of superhelical DNA.

We have presented here a realistic and computationally feasible model that includes both elastic and electrostatic energy components. The elastic bending and twisting potentials are controlled by bending and torsional rigidity force constants, formulated from local fluctuations of bending and twisting angles. Only the nonelectrostatic contribution of the bending fluctuations to the persistence length is considered because the electrostatic interactions are treated separately. The Debye-Hückel electrostatic potential developed here has salt-dependent coefficients, derived from Stigter's analysis of charged cylinders that produced effective DNA diameters as a function of salt in excellent agreement with experiment. This potential is expected to produce more realistic results than an uncharged model but is still clearly a crude approximation. Improved potentials that reflect the directly measured ionic strength-dependent forces between DNA helices in ordered arrays (Podgornik et al., 1994) may provide an even better description of supercoiled DNA in the future. Ultimately, of course, proteins should be modeled to mimic the natural environment realistically.

Our detailed computational study at salt concentrations ranging from 0.005 to 1.0 M sodium reveals that configurations and energies of supercoiled DNA change dramatically with salt. The quantitative data offered here complement the current capabilities of low resolution experiments. At high salt, the DNA is tightly interwound, very compact, and highly bent (Figs. 10 *e* and 16). Indeed, the simulated tight supercoiling with interwound segments in close contact agrees well with the cryo-electron microscopy data (Bednar et al., 1994). These geometries did not emerge in previous Monte Carlo simulations carried out in that work. This may be because of both the polygonal representation of the DNA and the stiff nonbonded potential mentioned above. Even when entropic effects are accounted for in our MD simulations, close contacts emerge often at high salt. Such close interactions within interwound superhelices of DNA have been suggested as an important functional state of DNA (Bednar et al., 1994). Further attractive interactions can be envisioned for divalent ions, such as magnesium, where electrostatic screening is much stronger (Shaw and Wang, 1993; Stighter and Dill, 1993; Adrian et al., 1990; Timsit and Moras, 1991; Timsit et al., 1989). The electrostatic energies remain roughly constant as superhelical density changes at high salt, and thus the competition between the bending and twisting terms determines the favorable configurations. At low salt, strong resistance to supercoiling prevails, and the DNA forms are very open and loosely supercoiled.

Thus, overall, at high salt the bending and twisting energies are the dominant terms that determine DNA configuration, and the electrostatic component plays a minor role. At low salt, the electrostatic component plays a much greater role. Because repulsion is greater at low salt and limits more severely the acceptable writhing numbers for the DNA, E_T is greater for low salt for a given ΔLk. Overall, the total supercoiling energy increases quadratically with ΔLk at all salt environments.

The overall geometric trends can be seen from Fig. 22, where the writhing numbers and the ratios $Wr/\Delta Lk$ are shown at five salt concentrations for a 1000 bp DNA with A/C = 1.5. These curves are drawn from the data presented earlier (Figs. 2–5) and additional studies (at 0.2 and 0.05 M concentrations). Only the families beginning with the figure-8 ($Wr \approx 1$) are shown. We clearly note that larger writhing numbers and greater number of families are attained at higher salt. Interestingly, the overall slopes in the Wr vs. ΔLk plot are quite similar. At the extreme low salt (0.005 M), note that only the figure-8 family is observed up to $\Delta Lk = 6$; it emerges with $Wr \approx 0.6$, unlike at higher salts, where Wr is closer to one. This low salt environment is clearly an extreme one, where the effective diameter of the DNA is about 225 Å. Furthermore, with a higher torsional rigidity elastic constant, which might be more appropriate, the slopes will consistently shift for all salts. Note from Fig. 22 how salt affects the partitioning of superhelicity between writhe and twist. At low salt, a much smaller fraction of the torsional strain is absorbed into writhing. Similarly, this fraction is much lower for the lobed than the linear interwound forms.

No toroidal forms resembling those suggested by small-angle x-ray scattering profiles at low salt (Brady et al., 1983,

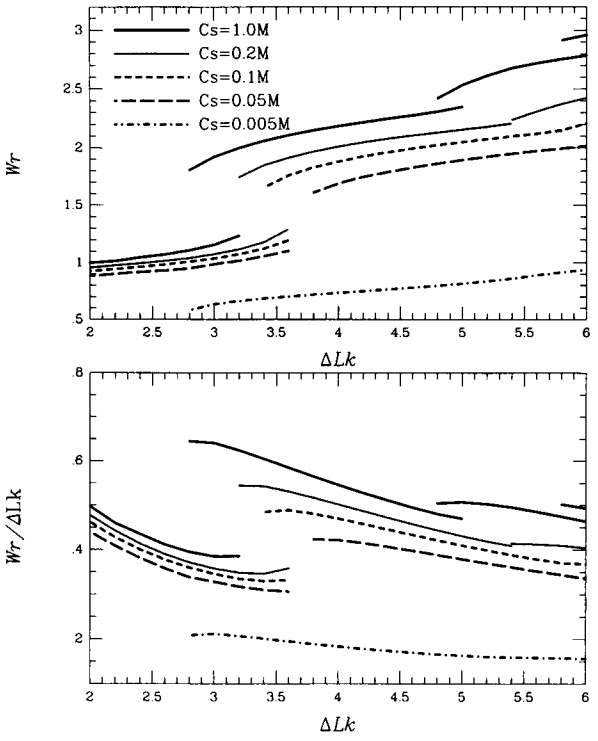

FIGURE 22 A summary of salt effects on minimized Wr and $Wr/\Delta Lk$ for 1000 base pairs, $A/C = 1.5$. For the five salt environments examined in this work, characteristics of the families beginning with the figure-8 forms identified by minimization are shown as a function of ΔLk. Bending, twisting, and electrostatic energy components are employed as described in the text.

1987) have been identified in this work. However, the circular, loosely coiled structures characteristic at low salt are more similar in overall dimensions to the toroidal configurations than to the long and thin shapes of interwound supercoils. This interpretation has also been offered by Bednar et al. (1994). Although increased branching at lower salt may lead to larger radii of gyration in long supercoiled chains (Bednar et al., 1994), the lobed forms (closely related to branched supercoils) generated here might account for these trends in smaller plasmids and loops.

To test this hypothesis, we generated x-ray intensity profiles from minima identified at different salt concentrations with superhelical densities similar to experimental conditions ($|\sigma| = 0.05$) (see legend for details). Fig. 23 shows these profiles for the linear interwound and lobed families of structures. We clearly note the same overall salt-dependent trends in the profiles of the linear interwound forms as those observed experimentally. Specifically, as salt is lowered, a pronounced maximum emerges as the supercoiling becomes looser. Furthermore, the position of the maximum remains approximately the same, as in the experimental profiles. Note also the dramatic change in the profiles as salt decreases below 0.1 M. The lobed profiles reveal more regular patterns with more than one peak, arising from the special symmetry in the structures. A systematic shift in intensity maxima is again observed as salt concentration decreases, with a particularly large shift below 0.1 M. Clearly, none of these profiles is consistent with an idealized, regular superhelical structure, which has very high peaks corresponding to regular intersegmental separation. Thus, the geometric difference between tightly closed and open structures, rather than between interwound and toroidal forms, can account for the observed scattering patterns (Brady et al., 1983, 1987) as a function of ionic environment.

In this connection, the identification of the three-lobed DNA family and exploration of its geometric and energetic details is another novel result. The three-lobed forms are expected to be stable according to elasticity theory but to our knowledge have not been obtained by computational methods and associated with DNA structure. Although energetically similar at low salt, the overall shapes of the lobed and interwound forms are quite different. Compare for example, the lobed family at $c_s = 0.005$ M (see Figs. 14 and 15) and the interwound minima (figure-8) in Fig. 10. The emergence of the lobed forms at low salt during the dynamics trajectory further suggests the possible biological relevance of these forms.

Another important consequence of these studies is direct evidence that the branched interwound is a member of the lobed family. The evolution of this family has been captured by the minimization analyses. The existence of critical ΔLk values for each salt environment where the lobed family members branch (e.g., $\Delta Lk = 4.6$ for 1.0 M, $\Delta Lk = 7$ for 0.1 M), to result in a branched interwound structure, for example, might be related to biological activities of supercoiled DNA. One might imagine a protein-binding mechanism associated with the opening of the lobes near a critical ΔLk value, as has been suggested for supercoiled-directed trefoil knotting (Schlick and Olson, 1992b). The unique open geometries offered by members of the lobed family—not unlike trefoils—offer DNA-binding proteins, such as topoisomerases, the right geometry for anchoring themselves onto the DNA, carrying out their function, and releasing themselves when their mission is complete.

The data presented here also suggest that the effects of salt on DNA structure and dynamics are highly nonlinear. At $c_s = 0.1$ M, the buckling transition from the circle to the figure-8 corresponds to a critical value; at lower concentrations, this transition is sharply delayed. Above 0.1 M concentrations at physiological densities there also appears to be a dramatic change from loose to very compact (although rather rigid) structures. This behavior is supported by the experimental data and Monte Carlo simulations of Bednar et al. (1994). The major difference in flexibility appears to arise from the geometric characteristics at the different salt environments.

Such distinct trends in DNA flexibility as a function of salt emerge from the dynamics trajectories and provide further information on this critical concentration. At high salt, we find the DNA to be tightly wound but fairly rigid, whereas at very low salt the chain is open but flexible because of strong repulsive interactions. From the data of Table 3, we deduce that at $c_s = 1.0$ M, fluctuations occur among the nearby F2, F3, and F4 families (Fig. 2 *a*), whereas at $c_s =$

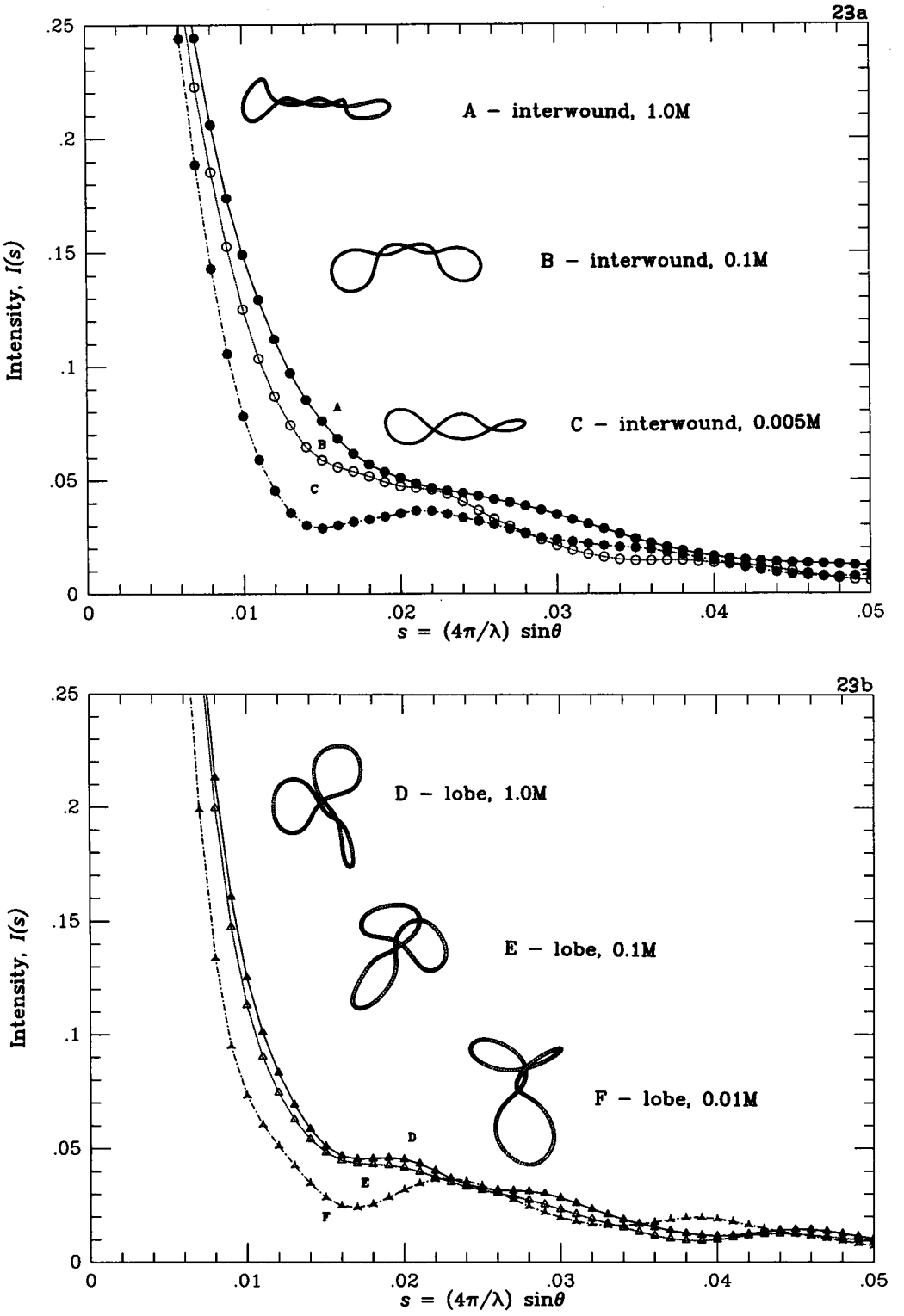

FIGURE 23 X-ray scattering profiles corresponding to minimized interwound (*a*) and lobed (*b*) forms at different salt concentrations, 1000 base pairs, $\Delta Lk = 5.5$. The chosen superhelical density corresponds to that of the native supercoiled COP608 plasmids used by Brady and co-workers in low-angle x-ray scattering experiments (Brady et al. 1983, 1987). The scattering profiles are computed here by a discrete form of the Debye integral (see, for example, Kirste, 1967). In discrete form, $I(s) = I(0)\,\Sigma_{i<j}\{\sin(x)/x\}$, where $x = sr_{ij}$, $s = (4\pi/\lambda)\sin\theta$, and the normalization factor is the inverse of the number of terms in the summation. The variables r_{ij} denote the pairwise distances along the DNA; s is in units of inverse length; λ is the wavelength (1.54 Å according to Brady and co-workers); and θ is one half the scattering angle.

0.005 M, only the F1 family is sampled (Fig. 4 *a*). At intermediate salt near physiological values (0.1 M), the extended F2 family is sampled along with some configurations very close to F1 (Fig. 3 *a*). The competition among the entropic, electrostatic, and elastic forces produces the greatest flexibility overall at this critical concentration. In this environment, the DNA is more dynamic and adopts a wider range of configurations and energies. This might be explained by a critical relationship between the effective diameter of the DNA and the persistence length at physiological concentrations. The experimental observations regarding increased branching at lower salt (Bednar et al., 1994) are consistent with these findings.

As suggested here and in Bednar et al. (1994), the observed relationships between salt and supercoiled DNA properties may be important for key regulatory processes, such as recombination and transcription, which require the DNA to be in favorable configurational and dynamical states. Indeed, many cellular or recognition interactions are known to be salt-sensitive. The results here demonstrate that the salt environment can act to regulate the onset of supercoiling, the collapse to the interwound, and the branching of DNA. These, in turn, will influence key biological functions. Furthermore, such relationships between salt and DNA structure extend beyond supercoiled DNA; they also apply to short spatially constrained segments of DNA that may occur throughout the genome. In this connection, the trends with respect to supercoiling tendencies as a function of chain length reveal the strong bending resistance to supercoiling for shorter chains, especially at low salt. This resistance, in turn, suggests a critical regulatory role for salt on functions of small looped segments of DNA, particularly in connection with DNA-binding proteins. Nonetheless, still be to be explored in this regard are effects of DNA crowding in the cell and the connection between in vivo and in vitro environments. If indeed certain processes, such as protein binding to DNA in *Escherichia coli*, are sensitive to salt concentration in vitro but not in vivo (Richey et al., 1987), the systematic results offered here indicate that some crucial biological mechanism must be unveiled to explain such intriguing experimental observations.

We thank Nathan Hunt, John Hearst, Gerald Manning, Irwin Tobias, Alex Vologodskii, and James Wang for valuable discussions and for sharing the results of recent work, Attilio De Falco and Andrew Olson for assistance with computer graphics, and one reviewer for pointing us to important experiments.

Our research was generously supported by the National Science Foundation (CHE-9002146, PYI Award ASC-9157582, and *Grand Challenge Award* ASC-9318159, the latter co-funded by ARPA), the U.S. Public Health Service (GM-34809), National Institutes of Health (CI-0474), the Searle Scholars Program/The Chicago Community Trust, the Whitaker and Sloan Foundations, and the Howard Hughes Medical Institute.

REFERENCES

Adrian, M., B. H. Bordier, W. Wahli, A. Z. Stasiak, A. Stasiak, and J. Dubochet. 1990. Direct visualization of supercoiled DNA molecules in solution. *EMBO J.* 9:4551–4554.

Anderson, C. F., and W. Bauer. 1978. Supercoiling in closed circular DNA: dependence upon ion type and concentration. *Biochemistry.* 17:594–601.

Baikalov, I., K. Grzeskowiak, K. Tanagi, J. Quintana, and R. E. Dickerson. 1993. The crystal structure of the trigonal decamer C-G-A-T-C-G-6MeA-T-C-G: a B-DNA helix with 10.6 base-pairs per turn. *J. Mol. Biol.* 231: 768–784.

Bartels, R. H., J. C. Beatty, and B. A. Barsky. 1987. An Introduction to Splines for Use in Computer Graphics & Geometric Modeling. Morgan Kaufmann, Los Altos, CA.

Bauer, W. R., R. A. Lund, and J. H. White. 1993. Twist and writhe of a DNA loop containing intrinsic bends. *Proc. Natl. Acad. Sci. USA.* 90:833–837.

Bednar, J., P. Furrer, A. Stasiak, J. Dubochet, E. H. Engelman, and A. D. Bates. 1994. The twist, writhe and overall shape of supercoiled DNA change during counterion-induced transition from loosely to a tightly interwound superhelix. Possible implications for DNA structure in vivo. *J. Mol. Biol.* 235:825–847.

Benham, C. J. 1989. Onset of writhing in circular elastic polymers. *Phys. Rev. A.* 39:2852–2856.

Berman, H. M., W. K. Olson, D. L. Beveridge, J. Westbrook, A. Gelbin, T. Demeny, S.-H. Hsieh, A. R. Srinivasan, and B. Schneider. 1992. The nucleic acid database: a comprehensive relational database of three-dimensional structures of nucleic acids. *Biophys. J.* 63:751–759.

Boles, T. C., J. H. White, and N. R. Cozzarelli. 1990. Structure of plectonemically supercoiled DNA. *J. Mol. Biol.* 213:931–951.

Brady, G. W., D. B. Fein, J. Lambertson, V. Grassian, D. Foos, and C. J. Benham. 1983. X-ray scattering from the superhelix in circular DNA. *Proc. Natl. Acad. Sci. USA.* 80:741–744.

Brady, G. W., M. Satkowski, D. Foos, and C. J. Benham. 1987. Environmental influences on DNA superhelicity. The effect of ionic strength on superhelix conformation in solution. *J. Mol. Biol.* 195:185–191.

Campbell, A. M. 1976. The effects of deoxyribonucleic acid secondary structure on tertiary structure. *Biochem. J.* 159:615–620.

Chirico, G., and J. Langowski. 1992. Calculating hydrodynamic properties of DNA through a second-order Brownian dynamics algorithm. *Macromolecules.* 25:769–775.

Dubochet, J., M. Adrian, J.-J. Chang, J. C. Homo, J. Lepault, A. W. McDowall, and P. Schultz. 1988. Cryo-electron microscopy of vitrified specimens. *Q. Rev. Biophys.* 21:129–228.

Fenley, M. O., W. K. Olson, I. Tobias, and G. S. Manning. 1994. Electrostatic effects in short superhelical DNA. *Biophys. Chem.* 50: 255–271.

Fuller, F. B. 1971. The writhing number of a space curve. *Proc. Natl. Acad. Sci. USA.* 68:815–819.

Greengard, L. 1988. The Rapid Evaluation of Potential Fields in Particle Systems. MIT Press, Cambridge, MA.

Hagerman, P. J. 1988. Flexibility of DNA. *Annu. Rev. Biophys. Biophys. Chem.* 17:265–286.

Hao, M.-H., and W. K. Olson. 1989a. Modeling DNA supercoils and knots with B-spline functions. *Biopolymers.* 28:873–900.

Hao, M.-H., and W. K. Olson. 1989b. Global equilibrium configurations of supercoiled DNA. *Macromolecules.* 22:3292–3383.

Hasted, J. B. 1973. Aqueous Dielectrics. Chapman and Hall, London.

Hearst, J. E., and N. G. Hunt. 1991. Statistical mechanical theory for the plectonemic DNA supercoil. *J. Chem. Phys.* 95:9322–9327.

Heinemann, U., C. Alings, and M. Bansal. 1992. Double helix conformation, groove dimensions, and ligand binding potential of a G/C stretch in B-DNA. *J. Mol. Biol.* 210:369–381.

Hunt, N. G., and J. E. Hearst. 1991. Elastic model of DNA supercoiling in the infinite-length limit. *J. Chem. Phys.* 95:9329–9336.

Jolly, D. J., and A. M. Campbell. 1972. The three-dimensional structure of supercoiled deoxyribonucleic acid in solution. *Biochem. J.* 128:569–578.

Kirste, R. G. 1967. Scattering functions of polymer coils. *In* Small Angle X-Ray Scattering. H. Brumberger, editor. Gordon and Breach, New York. 33–62.

Klenin, K. V., A. V. Vologodskii, V. V. Anshelevich, A. M. Dykhne, and M. D. Frank-Kamenetskii. 1988. Effect of excluded volume on topological properties of circular DNA. *J. Biomol. Struct. Dyn.* 5:1173–1185.

Klenin, K. V., A. V. Vologodskii, V. V. Anshelevich, A. M. Dykhne, and M. D. Frank-Kamenetskii. 1991. Computer simulation of DNA supercoiling. *J. Mol. Biol.* 217:413–419.

Klenin, K. V., A. V. Vologodskii, V. V. Anshelevich, V. Y. Klisko, A. M. Dykhne, and M. D. Frank-Kamenetskii. 1989. Variance of writhe for wormlike DNA rings with excluded volume. *J. Biomol. Struct. Dyn.* 6:707–714.

Lipanov, A., M. L. Kopka, M. Kaczor-Grzeskowiak, J. Quintana, and R. E. Dickerson. 1992. Structure of the B-DNA decamer C-C-A-A-C-I-T-T-G-G in two different space groups: conformational flexibility of B-DNA. *Biochemistry.* 32:1373–1389.

Livolant, F., A. M. Levelut, J. Doucet, and J. P. Benoit. 1989. The highly concentrated liquid-crystalline phase of DNA is columnar hexagonal. *Nature.* 339:724–726.

Love, A. E. 1944. Treatise on the Mathematical Theory of Elasticity, 4th ed. Dover, New York.

Manning, G. S. 1978. The molecular theory of polyelectrolyte solutions with applications to the electrostatic properties of polynucleotides. *Q. Rev. Biophys.* 179:181–246.

Manning, G. S. 1981. A procedure for extracting persistence lengths from light-scattering data on intermediate molecular weight DNA. *Biopolymers.* 20:1751–1755.

Manning, G. S. 1988. Three persistence lengths for a stiff polymer with an application to DNA B-Z junctions. *Biopolymers.* 27:1529–1542.

Le Bret, M. 1979. Catastrophic variation of twist and writhing of circular DNAs with constraint? *Biopolymers.* 18:1709–1725.

Le Bret, M. 1984. Twist and writhing in short circular DNAs according to first-order elasticity. *Biopolymers.* 23:1835–1867.

Olson, W. K., and P. Zhang. 1991. Computer simulation of DNA supercoiling. *In* Methods in Enzymology, Vol. 203, Molecular Design and Modeling: Concepts and Applications, Part B, Antibodies and Antigens, Nucleic Acids, Polysaccharides, and Drugs. J. J. Langone, editor. Academic Press, Orlando, FL. 403–432.

Olson, W. K., Babcok, M. S., Gorin, A., Liu, G-H., Marky, N. L., Martino, J. A., Pedersen, S. C., Srinivasan, A. R., Tobias, I., Westcott, T. P., and Zhang, P. 1994. Flexing and folding double helical DNA. *Biophys. Chem.* In press.

Podgornik, R., D. C. Rau, and V. A. Parsegian. 1994. Parameterization of direct and soft steric-undulatory forces between DNA double helical polyelectrolytes in solutions of several different anions and cations. *Biophys. J.* 66:962–971.

Ramachandran, G., and T. Schlick. 1994. Enhanced flexibility of supercoiled DNA due to interactions. Preprint.

Richey, B., D. S. Cayley, M. C. Mossing, C. Kolka, C. F. Anderson, T. C. Farrar, and M. T. Record. 1987. Variability of the intracellular ionic environment of *escherichia coli.* Differences between in vitro and in vivo effects of ion concentration on protein-DNA interactions and gene expression. *J. Biol. Chem.* 262:7157–7164.

Rybenkov, V. V., N. R. Cozzarelli, and A. V. Vologodskii. 1993. Probability of DNA knotting and the effective diameter of the DNA double helix. *Proc. Natl. Acad. Sci. USA.* 90:5307–5311.

Schlick, T., B. Li, and M.-H. Hao. 1994. Calibration of the timestep for molecular dynamics of supercoiled DNA modeled by B-splines. *In* Structural Biology: State of the Art 1993, Proceedings of the Eighth Conversations, Vol. 1. R. H. Sarma and M. H. Sarma, editors. Adenine Press, Schenectady, NY. 157–174.

Schlick, T., and W. K. Olson. 1992a. Supercoiled DNA energetics and dynamics by computer simulation. *J. Mol. Biol.* 223:1089–1119.

Schlick, T., and W. K. Olson. 1992b. Trefoil knotting revealed by molecular dynamics simulations of supercoiled DNA. *Science.* 257:1110–1115.

Schlick, T., W. K. Olson, T. Westcott, and J. P. Greenberg. 1994. On higher buckling transitions in supercoiled DNA. *Biopolymers.* 34:565–598.

Shaw, S. Y. and J. C. Wang. 1993. Knotting of a DNA chain during ring closure. *Science.* 260:533–536.

Shimada, J., H. Kaneko, and T. Takada. 1994. Performance of fast multipole methods for calculating electrostatic interactions in biomolecular simulations. *J. Comp. Chem.* 15:28–43.

Song, L., B. S. Fujimoto, P. Wu, J. C. Thomas, J. H. Shibata, and J. M. Schurr. 1990. Evidence for allosteric transitions in secondary structure induced by superhelical stress. *J. Mol. Biol.* 241:307–326.

Spengler, S. J., A. Stasiak, and N. R. Cozzarelli. 1985. The stereostructure of knots and catenanes produced by phage λ integrative recombination: implications for mechanism and DNA structure. *Cell.* 42:325–334.

Sprous, D., R. K.-Z. Tan, and S. C. Harvey. 1994. Molecular modeling of closed circular DNA thermodynamic ensembles. Preprint.

Stigter, D. 1977. Interactions of highly charged colloidal cylinders with applications to double-stranded DNA. *Biopolymers.* 16:1435–1448.

Stigter, D., and K. A. Dill. 1993. Theory for second virial coefficients of short DNA. *J. Phys. Chem.* 97:12995–12997.

Tan, R. K.-Z., and S. C. Harvey. 1989. Molecular mechanics model of supercoiled DNA. *J. Mol. Biol.* 205:573–591.

Tan, R. K.-Z., and S. C. Harvey. 1991. Succinct macromolecular models: application to supercoiled DNA. *In* Theoretical Biochemistry and Molecular Biophysics, Vol. 1. R. Lavery, & D. Beveridge, editors. Adenine Press, Schenectady, NY. 125–137.

Taylor, W. H., and P. J. Hagerman. 1990. Application of the method of phage T4 DNA ligase-catalyzed ring-closure to the study of DNA structure. II. NaCl-dependence of DNA flexibility and helical repeat. *J. Mol. Biol.* 212:363–376.

Tesi, M. C., E. J. J. van Rensburg, E. Orlandini, D. W. Sumners, and S. G. Whittington. 1994. Knotting and supercoiling in circular DNA: a model incorporating the effect of added salt. *Phys. Rev. E.* 49:868–872.

Timsit, Y., and D. Moras. 1991. Groove-backbone interaction in B-DNA—implication for DNA condensation and recombination. *J. Mol. Biol.* 221: 919–940.

Timsit, Y., E. Vilbois, and D. Moras. 1991. Base-pairing shift in the major groove of $(CA)_n$—tracts by B-DNA crystal structures. *Nature.* 354:167–170.

Timsit, Y., E. Westhof, R. P. P. Fuchs, and D. Moras. 1989. Unusual helical packing in crystals of DNA bearing a mutation hot spot. *Nature.* 341: 459–462.

Tsuru, H., and M. Wadati. 1986. Elastic model of highly supercoiled DNA. *Biopolymers.* 25:2083–2096.

Vologodskii, A. V., V. V. Anshelevich, A. V. Lukashin, and M. D. Frank-Kamenetskii. 1979. Statistical mechanics of supercoils and the torsional stiffness of the DNA double helix. *Nature.* 280:294–298.

Vologodskii, A. V., and N. R. Cozzarelli. 1994. Conformational and thermodynamic properties of supercoiled DNA. *Annu. Rev. Biophys. Biomol. Struct.* 23:609–643.

Vologodskii, A. V., S. D. Levene, K. V. Klenin, M. D. Frank-Kamenetskii, and N. R. Cozzarelli. 1992. Conformational and thermodynamic properties of supercoiled DNA. *J. Mol. Biol.* 227:1224–1243.

Wang, J. C. 1969. Variation of the average rotation angle of the DNA helix and the superhelical turns of covalently closed cyclic λ DNA. *J. Mol. Biol.* 43:25–39.

White, J. H. 1969. Self-linking and the Gauss integral in higher dimensions. *Am. J. Math.* 91:693–728.

White, J. H. 1989. An introduction to the geometry and topology of DNA structures. *In* Mathematical Methods for DNA Sequences, Ch. 9 M. S. Waterman, editor. CRC Press, Boca Raton, FL. 225–253.

Yang, Y., I, Tobias, and W. K. Olson. 1993. Finite element analysis of DNA supercoiling. *J. Chem. Phys.* 98:1673–1686.

Zajac, E. E. 1962. Stability of two planar loop elasticas. *Trans. ASME, Ser. E, J. Appl. Mech.* 29:136–142.

Zhang, P., W. K. Olson, and I. Tobias. 1991. Accelerated record keeping Fourier series Monte Carlo simulations of an isotropic elastic rod model of DNA. *Comp. Polymer Sci.* 1:3–17.